STUDY OF THE INFLUENCE OF LEADING EDGE ROTATING CYLINDER ON THE PERFORMANCE OF A SYMMETRIC AEROFOIL

KH. MD. FAISAL
(BSc Engg., MIST)

A THESIS SUBMITTED FOR THE DEGREE OF

MASTER OF SCIENCE

DEPARTMENT OF MECHANICAL ENGINEERING

MILITARY INSTITUTE OF SCIENCE AND TECHNOLOGY (MIST)

MIRPUR CANTONMENT, DHAKA 1216, BANGLADESH

FEBRUARY 2017

The thesis titled "**STUDY OF THE INFLUENCE OF LEADING EDGE ROTATING CYLINDER ON THE PERFORMANCE OF A SYMMETRIC AEROFOIL.**" submitted by Kh. Md. Faisal, Roll No: 1014180010(F) Session: October 2014 has been accepted as satisfactory in partial fulfillment of the requirement for the degree of Master of Science on FEBRUARY 2017

NAME OF THE COMMITTEE MEMBERS WITH AFFILIATION

1 _____ Chairman

Dr. M A Taher Ali,
Professor
Department of Aeronautical Engineering, MIST.

2 _____ Member

Brig. Gen. Md Lutfor Rahman, Ph. D. (Ex-officio)
Senior Instructor & Head
Department of Mechanical Engineering, MIST.

3 _____ Member

Prof. Dr. Mohammad Ali
Head of the Department
Department of Mechanical Engineering, BUET

4 _____ Member

Wg. Cdr. Vikram V. Deshpande, Ph.D.
Instructor Class A
Department of Aeronautical Engineering, MIST.

DECLARATION

I hereby declare that this thesis is my original work and it has been written by me in its entirety. I have duly acknowledged all the sources of information which have been used in the thesis.

This thesis has also not been submitted for any degree in any university previously.

_____

Kh. Md. Faisal

February, 2017

ACKNOWLEDGEMENT

I wholeheartedly thank my supervisor Prof. Dr. M. A. Taher Ali, whose guidance, insight and instruction was the main essence of this study and without which the study would not be possible.

I thank respected head of the Department of Mechanical Engineering, MIST, Brig Gen Md. Lutfor Rahman, PhD to give me the permission to use Machine Tools Lab as well as Workshop of Mechanical Engineering Department.

Again I heartily thank the Head of the Department of Aeronautical Engineering, Group Captain Md. Abdus Salam, Bangladesh Air Force for providing me with opportunities and facilities of the office and the laboratory to conduct this thesis.

Wing Commander Dr. Vikram V. Deshpande, Indian Air Force, Instructor Class-A of Department of Aeronautical Engineering, MIST extended his guidance throughout the whole process for CFD simulation. I want to express my gratitude for his valuable time and relentless inspiration.

I want to express my gratitude towards Mr. Dibakar Tarafdar whose valuable craftsmanship made excellent contributions to the test section modification and manufacturing of newly developed setup. These works are valuable assets of this study. I thank Mr. Aminul Islam who helped me for assembly and disassembly of different parts as required during carrying out the experiments.

TABLE OF CONTENTS

ABSTRACT

This research dealt with moving surface boundary layer control, applied to NACA 0018 aerofoil both by simulation and experiment. The moving surface was provided by a rotating cylinder placed at the leading edge of the aerofoil.

In aeronautics, Reynolds number 10^5 constitutes an important speed regime as many unmanned aerial vehicle operates in this regime. But little work was done in this field. Thus, this research aims for investigation of aerofoil performance having rotating cylinder at the leading edge in the Reynolds number range of 10^5 regime. For conducting this research on a symmetric aerofoil, NACA 0018 was chosen. Experimental data on NACA 0018 aerofoil at Reynolds number 2.4 X 10^5 were obtained from existing literature. The set of data was taken and simulations were done on the same aerofoil with different models like k-ω SST, Spalart Almaras. It was found that data obtained by k-ω SST model were close to experimental data. Thus in the present investigation simulations were done using this model in ANSYS. Performance of NACA 0018 were investigated and data from the modified NACA 0018 aerofoil was obtained at four different Reynolds number 1.4 X 10^5 to 2.8 X 10^5 with zero rpm and five other rpm starting from 3000 to 5000 with the interval of 500. Results obtained through experiment were then compared with the simulation data of NACA 0018 aerofoil. This comparison showed that at lower Reynolds number (at 1.4 X 10^5 & 1.85 X 10^5) stall was delayed as well as maximum lift coefficient was increased while at Reynolds number 2.3 X 10^5 stall was delayed without any increment in maximum lift coefficient. Finally at Reynolds number 2.8 X 10^5 stall was little delayed with a slight decrease in maximum lift coefficient because of increase in velocity ration as well as vibration.

LIST OF FIGURES

LIST OF TABLES

NOMENCLATURE

F_L	lift force
F_D	drag force
N	normal force
A	axial force
α	angle of attack
M	moment
TE	trailing edge
LE	leading edge
p	local pressure
q_∞	dynamic pressure
V_∞	free stream velocity
ρ_∞	free stream air density
C_L	coefficient of lift
C_D	coefficient of drag
C_{Lmax}	maximum coefficient of lift
R	radius
Ø	diameter
Re	Reynolds number

CHAPTER 1

INTRODUCTION

One of the most important factor for flying an aerial vehicle is the amount of lift generated during flying. The generation of lift depends mainly on the nature of deflection of the free stream air, which in turn depends on the orientation of the aerofoil and its curved shape. Other factors are surface area and its roughness. Magnitude of relative free stream velocity is another main factor as it determines the flow separation causing stall. Boundary layer suction is one way to delay flow separation on the upper surface of the aerofoil in order to delay stall which increases lift to drag ratio. Lift to drag ratio of an aerofoil is optimized by carefully considering all the above factors in the design process of an aerofoil. Attempts are being made to incorporate some extra devices with the wing to increase its lift to drag ratio. Researches are being carried out in this line by incorporating a rotating cylinder at the leading edge of the aerofoil in order to utilize Magnus effect to increase the lift with minimum influence on its drag. In this research the experimental study are carried out on NACA 0018 aerofoil by incorporating a rotating cylinder on its leading edge. The experiment was carried out in the existing wind tunnel (ArmField-100 TQ 052524-02) of the laboratory. Some of the results thus obtained were verified with those obtained from some analysis tools.

The first section of this chapter provides with the description of aerofoil, then some analysis of aerodynamic forces including Magnus effect acting on aerofoil in understanding its lift characteristics in different flow conditions and orientations.

1.1 Aerofoil

An aerofoil is the cross-sectional shape of a wing or a sail or blade (of a propeller, a rotor or a turbine). An aerofoil-shaped body when moved through a fluid produces an aerodynamic force. The component of this force perpendicular to the direction of motion is called lift and that parallel to the direction of motion is called drag. Subsonic flight aerofoils have a characteristic shape of a round leading edge, followed by a sharp trailing edge, often with asymmetric camber. Aerofoils of similar function designed for water as the working fluid are called hydrofoils.

The lift on an aerofoil is primarily depends on its angle of attack and shape. When oriented at a suitable angle, the aerofoil deflects the oncoming air, producing a force in the direction opposite to the deflection of motion. This force is known as aerodynamic force which can be resolved into two components: one parallel to the flow direction and other perpendicular to it. The parallel component produces drag and the perpendicular one lift. Most aerofoil shapes require a positive angle of attack to generate lift, but cambered Aerofoils can generate lift at zero angle of attack because of its profile curvature. The deflection of free stream air velocity results in lower pressure on upper surface and higher pressure on lower surface. This pressure difference causes the upward force which is known as lift.

1.2 Various Aspects of Aerofoil

An Aerofoil is essentially a streamlined curved body producing differential pressure on its two sides in the fluid stream and is used extensively in many engineering applications. In the field of flying mainly it is used as the wings of aeroplanes producing lift and enables them to fly.

Purpose

All aerofoils are designed to deflect the free stream air and subsequently influence the performance of aeroplanes, car, boat or other object they are attached to. Aeroplanes don't just use them for lift; they use them to navigate right or left and sometimes as stabilizers. Racing cars often employ an upside down wing. These aerofoils press them toward the ground, keeping the car tight on the racing track, improving its traction. With all different types of aerofoils the common deign challenge is to increase lift while minimizing drag.

Leading Edge

Nearly all aerofoils have a relatively gentle radius at the leading edge forming a streamlined profile ending in narrow trailing edge. This curved profile causes less disruption as the aerofoil moves through the air. While the blunt head aerofoil produces vortex just near the corner producing drag, the streamlined aerofoil guides flow producing lift with minimum drag.

1.3 Types of Aerofoil

Aerofoils are of different shapes and sizes depending on the specifications and configuration of the intended aircraft.

There are three basic types of Aerofoils.

- Symmetrical Aerofoils
- Semi-symmetrical Aerofoils
- Flat Bottom Aerofoils

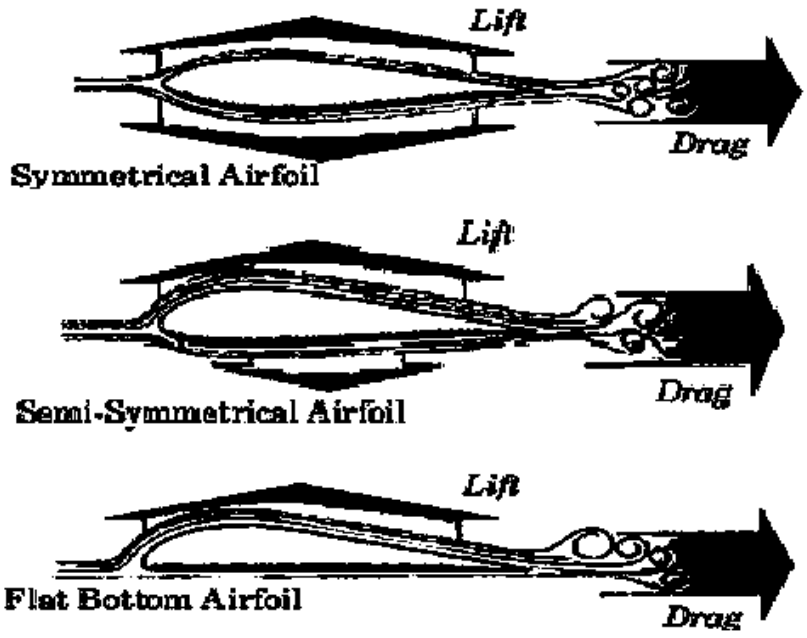

Figure 1.1 Three Basic types of Aerofoils

1.4 Terminologies of Aerofoil

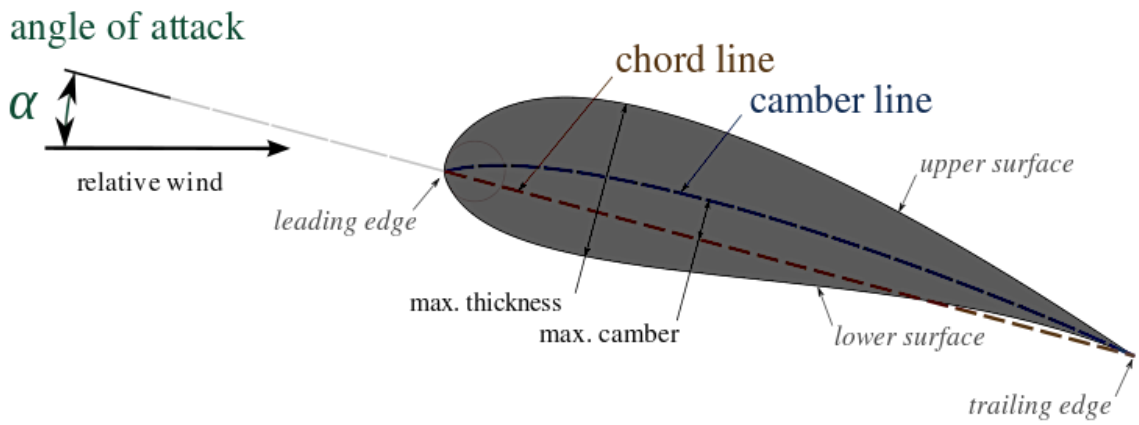

Figure 1.2 Aerofoil geometry

The various terms related to aerofoil:

The *mean camber line* is the line drawn midway between upper and lower surface.

The forward end point and rearward end points of mean camber line are called *leading edge and trailing edge* respectively.

The straight line connecting the leading edge and trailing edge is the *chord line* of the aerofoil.

The length of chord line is known as the chord.

Camber is the asymmetry between the top and the bottom surfaces of an aerofoil from its chord.

The thickness is the distance between upper and lower surface and measured perpendicular to the chord line.

1.5 Aerodynamic Forces

The aerodynamic forces and moment on an aerofoil or a body in general acting on a body may be described by *lift*, *drag* and *pitching moment*. *Lift* is the net vertical force and *drag* is the net horizontal force with respect to the direction of motion. The *pitching moment* reflects the tendency of the aerofoil to pitch about a given reference axis. These quantities are derived from the normal force and axial force acting on the aerofoil by trigonometric relations (Eq. 1 & 2)

$$F_L = N\cos\alpha - A\sin\alpha \quad (1)$$

$$F_D = A\cos\alpha + N\sin\alpha \quad (2)$$

The normal force (N) is defined as the force perpendicular to the aerofoil chord and the axial force (A) is the force acting parallel to the chord. It can be seen in these equations that the lift force (F_L) and the drag force (F_D) are both derived from the same normal and axial force. However, the angle of attack (α) determines how much of the normal and axial forces transfer into lift and how much into drag. The pitching moment may be expressed by an integral of the net moments acting on the aerofoil (Eq. 3).

$$M = \int_{LE}^{TE} dM_U + \int_{LE}^{TE} dM_L \quad (3)$$

In this equation, the differential moments are taken with respect to a given reference point and then integrated from the leading edge to the trailing edge. A graphical representation of these forces is shown in Figure 1.3

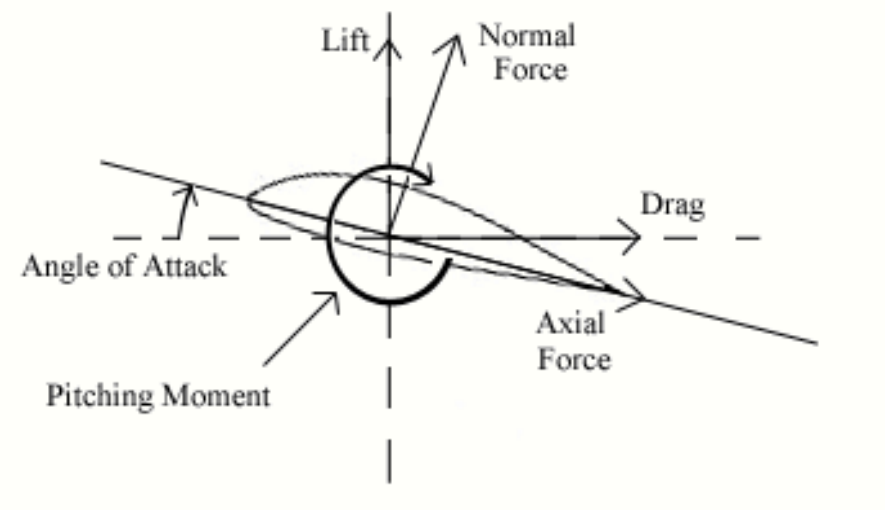

Figure 1.3 Aerodynamic forces

1.6 Low-Speed Aerodynamics

In low-speed flows, where the free stream velocity is well under Mach 0.3, several idealizations are applied to simplify fluid dynamics analysis. One such idealization is that the air density is assumed constant since it varies by only a few percent from speeds of 0 to 300 mph. This idealization is known as *incompressible* flow. Another idealization, *inviscid* flow, is made by neglecting viscous effects such as friction, thermal conduction and diffusion. Such effects are known to be minimal for low-speed air flow and this idealization is well supported by current theory. The flow is assumed to be steady, and the body forces acting on the working fluid are assumed to be minor compared to dynamic effects. These idealized conditions are sufficient to allow the use of Bernoulli's equation, (Eq. 4), in low-speed flow analysis.

Bernoulli's equation may also be derived from the momentum equation by considering a differential control volume and applying the assumptions as described above. The resulting equation shows that the sum of the local static pressure (p) and dynamic pressure (Eq. 5) are constant throughout a given flow. From this equation, the local velocities may be computed from knowledge of upstream data and local static pressure so that all of the flow characteristics may be obtained.

$$P + \frac{1}{2}\rho V_\infty^2 = \text{constant} = P + q_\infty \qquad (4)$$

$$q_\infty = \frac{1}{2}\rho V_\infty^2 \quad (5)$$

Effects of the wind tunnel walls may be ignored by applying the inviscid flow approximation. By doing so, the flow may be assumed to be uniform except around the aerofoil. Uniform flow simplifies control volume analysis, and allows the consideration of a full length aerofoil as a 2D profile. The assumption of uniform flow is justified due to the smooth wind tunnel walls and the controlled entry flow into the test section.

1.7 Characterizing Aerofoil Performance

Aerofoil performance may be characterized by quantities such as the lift, drag or pitching moment produced under different operating conditions. These aerodynamic forces are often computed from the total pressure over the planform area and then normalized by the dynamic pressure in order to produce non-dimensional quantities. For example, the lift coefficient may be expressed as (Eq. 6). The drag coefficients may also be expressed in a similar manner as (Eq. 7).

$$C_L \equiv \frac{F_L}{\frac{1}{2}\rho_\infty V_\infty^2 A} \quad (6)$$

$$C_D \equiv \frac{F_D}{\frac{1}{2}\rho_\infty V_\infty^2 A} \quad (7)$$

These non-dimensional quantities are functions of the Reynolds number and the angle of attack. The Reynolds number influence may be seen by the inclusion of the free stream air density (ρ_∞) and free stream velocity (V_∞) terms. While the angle of attack (AOA) influence is found through the force, moment and area terms. Thus to in order appreciate the full range of responses of a given aerofoil, it is necessary to consider a range of Reynolds numbers and angles of attack. Variation in the Reynolds number produces different lift curves, while variations in the angle of attack will alter the lift-drag ratio.

1.8 Magnus Effect

Gustav Magnus made experimental studies of the aerodynamic forces on spinning spheres and cylinders. These experiments led to the discovery of the Magnus Effect, which helps to explain the theory of lift.

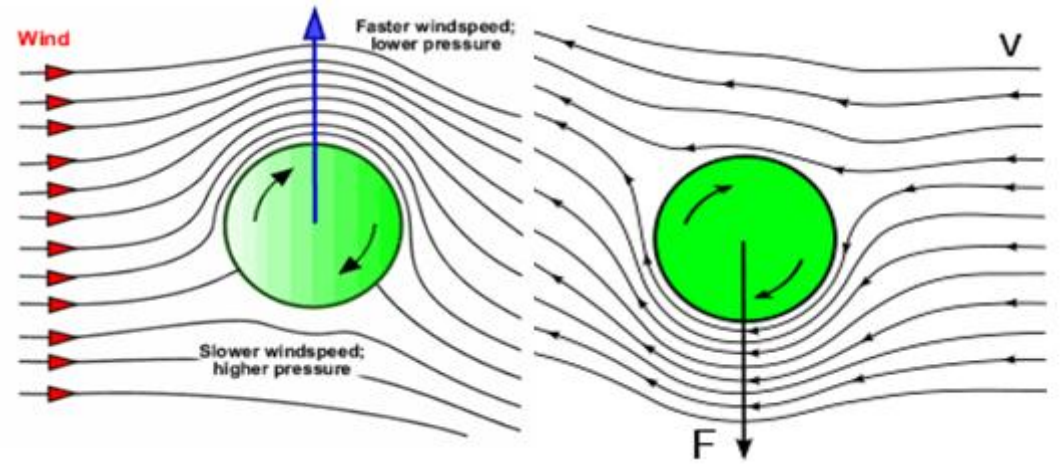

Figure 1.4 Magnus Effect

If a flow of air passes from left to right over a clockwise rotating cylinder as shown in Figure 1.4 then friction between fluid and the surface of the cylinder tends to drag the fluid near the surface in the same direction as rotational motion. As the air and surface of cylinder is moving in the same direction towards the upper surface so this "extra" velocity increases the velocity at the top while decreases at the bottom of the rotating cylinder. According to Bernoulli's equation as velocity increases pressure decreases so the pressure at the top surface is lower than the pressure on the lower surface. This pressure imbalance creates a net upward force, a finite lift. This phenomenon of generation of lift due to rotation of circular cylinder is known as Magnus effect [4]. Due to this Magnus effect, force will generate in downward direction if the direction of flow is reversed as shown in Figure 1.4

1.9 Boundary Layer and Reynolds Number

A commonly observed phenomena of fluid dynamics is that a fluid flowing over a surface has a very thin layer adjacent to the surface that sticks to it has a zero velocity. The next layer (or lamina) adjacent to the first has a very small velocity differential, relative to the first layer, whose magnitude depends on the viscosity of the fluid. The more viscous the fluid, the lower the velocity differential between each subsequent layer. At some distance δ, measured perpendicular to the surface, the velocity is equal to the free-stream velocity of the fluid. The distance δ is defined as the thickness of the boundary layer.

The boundary is composed of three regions beginning at the leading edge of a surface:

- The laminar region where each layer or lamina slips over the adjacent layer in an orderly manner creating a well-defined shear force in the fluid
- A transition region and
- A turbulent region where the particles of fluid mix with each other in a random way creating turbulence and eddies

The transition region is where the laminar region begins to become turbulent. The shear force in the laminar region and the swirls and eddies in the turbulent region both create drag, but with different physical processes. The cross-section of a typical boundary layer might look like Figure 1.5.

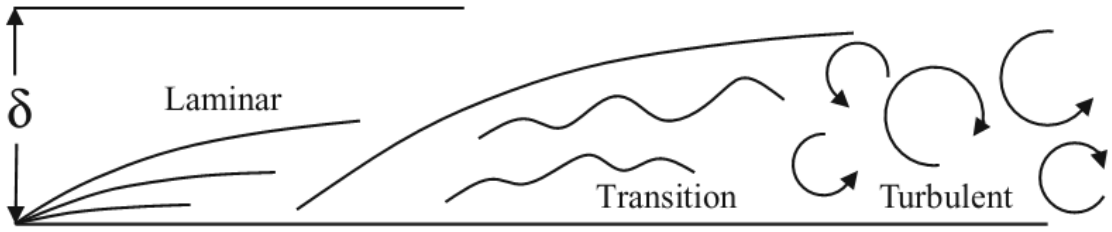

Figure 1.5 Typical Boundary Layer

The shearing stress that the fluid exerts on the surface is called skin friction and is an important component of the overall drag.

The two distinct regions in the boundary layer (laminar and turbulent) depend on the velocity of the fluid, the surface roughness, the fluid density, and the fluid viscosity. These factors, with the exception of the surface roughness, were combined by Osborne Reynolds in 1883 into a formula that has become known as the Reynolds number, which mathematically is expressed as:

$$R = \rho V \left(\frac{l}{\mu} \right) \tag{8}$$

where,

ρ is fluid density,

V is fluid velocity,

μ is fluid viscosity, and

l is a characteristic length.

In aeronautical work, the characteristic length is usually taken as the chord of a wing or tail. The Reynolds number is an important indicator of whether the boundary layer is in a laminar or turbulent condition. Laminar flow creates considerably less drag than turbulent but nevertheless causes difficulties with small surfaces.

Laminar flow causes drag by virtue of the friction between layers and is particularly sensitive to the surface condition. Normally, laminar flow results in less drag and is desirable. The drag of the turbulent boundary layer is caused by a completely different mechanism that depends on knowledge of Bernoulli's theorem. Bernoulli has shown that for an ideal fluid (no friction) the sum of the static pressure (P) and the dynamic pressure (q), where

$$q = \tfrac{1}{2}\rho V^2 \tag{9}$$

$$P + \frac{1}{2}\rho V^2 = \text{const.} \tag{10}$$

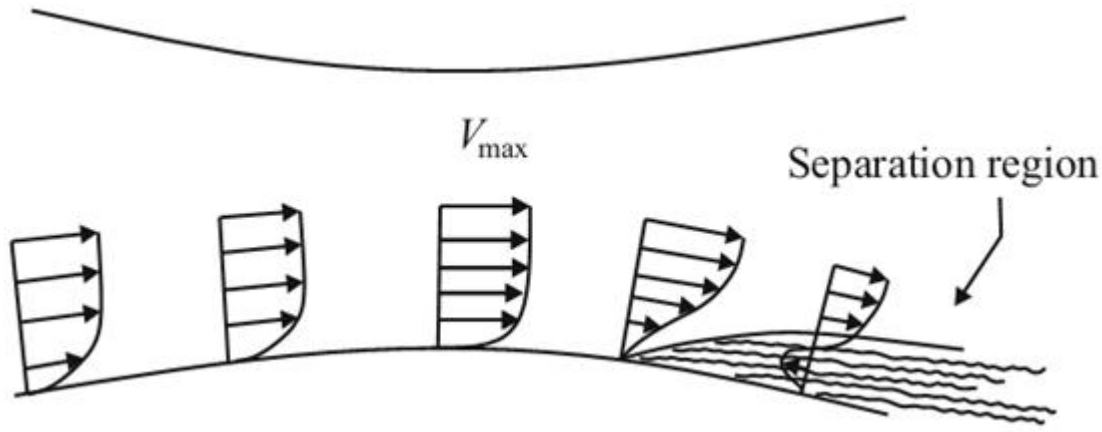

Figure 1.6 Boundary Layer Velocity Profile

Applying this principle to flow in a venturi, with the bottom half representing an airplane wing, the distribution of pressure and velocity in a boundary layer can be analyzed. As the fluid (assumed to be incompressible) moves through the venturi or over a wing, its velocity increases (because of the law of conservation of mass) and as a consequence of Bernoulli's theorem, its pressure decreases, causing what is known as

a favorable pressure gradient. The pressure gradient is favorable because it helps push the fluid in the boundary layer on its way. After reaching a maximum velocity, the fluid begins to slow and consequently forms an unfavorable pressure gradient (i.e., hinders the boundary layer flow) as seen by the velocity profiles in Figure 1.6. Small characteristic lengths and low speeds result in low Reynolds numbers and consequently laminar flow, which is normally a favorable condition. A point is reached in this situation where the unfavorable pressure gradient actually stops the flow within the boundary layer and eventually reverses it. The flow stoppage and reversal results in the formation of turbulence, vortices and in general a random mixing of the fluid particles. At this point, the boundary layer detaches or separates from the surface and creates a turbulent wake. This phenomenon is called separation and the drag associated with it is called pressure drag. The sum of the pressure drag and skin friction (friction drag—primarily due to laminar flow) on a wing is called profile drag. This drag exists solely because of the viscosity of the fluid and the boundary layer phenomena. Whether the boundary layer is turbulent or laminar depends on the Reynolds number, as does the friction coefficient, as shown in Figure 1.7

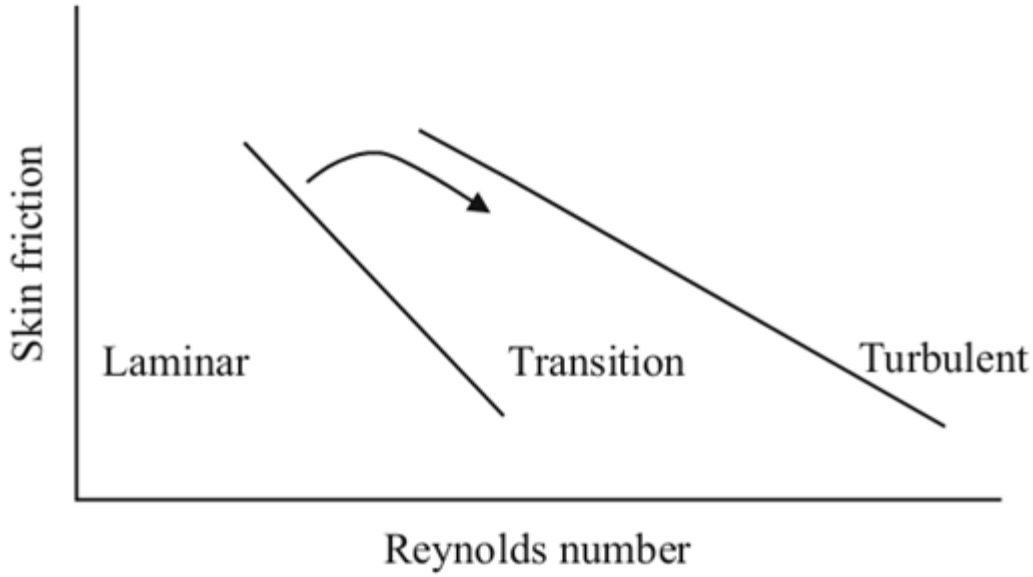

Figure 1.7 Skin friction Vs Reynolds Number

It would seem that laminar flow is always desired (for less pressure drag), and usually it is, but it can become a problem when dealing with very small UAVs that fly at low speeds. Small characteristic lengths and low speeds result in low Reynolds numbers and consequently laminar flow, which is normally a favorable condition. The favorable

and unfavorable pressure gradients previously described also exist at very low speeds, making it possible for the laminar boundary layer to separate and reattach itself. This keeps the surface essentially in the laminar flow region, but creates a bubble of fluid within the boundary layer. This is called laminar separation and is a characteristic of the wings of very-small, low-speed airplanes (e.g. small model airplanes and very small UAVs).

The Reynolds number is especially important for airfoil performance. This parameter determines the achievable section maximum lift coefficient and lift-to-drag ratio.

1.10 Objectives of Present Investigation

This research is targeted to achieve the objectives as stated below:

- Investigation of performance of symmetric aerofoil by simulation.
- Calibration of wind tunnel [ArmField-100 TQ 052524-02, the existing wind tunnel with MIST] and validation of wind tunnel data.
- Development of new experimental setup.
- Investigation of performance of symmetric aerofoil with leading edge rotating cylinder by newly developed experimental setup.
- Comparison of results of NACA 0018 aerofoil from simulation and results of modified NACA 0018 from experiment and drawing valid conclusions from this research.

CHAPTER 2

LITERATURE REVIEW

From initiation of human civilization transportation has been playing an important role in day to day life. Human endeavor was not stopped with the invention of the means of road transportation as well as water transportation. By means of these transportation systems, they started to enhance the communication system. In course of time there created a need for fast communication system which accelerated the development of automobile industry. But, human effort was not stopped at that point. People started to think of inventing a means of air transportation. Enough efforts were made in materializing this dream. Many people sacrificed their life in persuasion of this dream. After a lot of trials and failures, people started to gather learnings from those events and started to try in a different way. At this point of time, Wright brothers tried with different modes and methods. Ultimately they succeeded in 1903 when Wright brothers made their historic powered flight with the aircraft Wright Flyer-I [1]. Prior to their first successful flight they built an open loop wind tunnel of 6" X 6" test section. After building and testing the wind tunnel, the Wright brothers completed a larger, more sophisticated one in October 1901 [1]. They used it extensively to carry out aerodynamic research that proved essential in designing their 1903 airplane. Wilbur and Orville Wright conducted preliminary tests on as many as 200 different model wing shapes as they perfected the operation of their wind tunnel [2]. They made formal tests and recorded data on nearly 50 of these [3]. After that, NACA produced a lot of aerofoil with various camberness and thickness and assigned specific names to those aerofoils. In last 110 years technology has improved a lot. Different organizations/researchers have discovered different types of aerofoils. Today's aircrafts are highly sophisticated and are used both in civil and military purposes. But the requirement of finding a more aerodynamically efficient aerofoil has not yet been ended, rather it is associated with another major requirement of reducing the flying cost.

With blessings of technological development, researchers are searching for scopes to reduce the flying cost. This can be achieved mainly in three ways: developing efficient prime mover, reducing weight, by increasing the lift to drag ratio. Efficient prime mover is being developed day by day with advancement in engine technology. Weight reduction is achieved with the development of aerospace material. Improving the lift to drag ratio can be achieved with the development of aerodynamic performance of

aerofoil. Researchers in the field of aerodynamics are investigating ways to improve the lift to drag ratio which in turn will reduce the fuel requirement of an aircraft. Some recent trends are flapping wing, flying wing and others. Moreover, boundary layer suction, boundary layer blowing, vortex generator, boundary layer control etc. [4] are some of the ways of increasing the performance of aerofoil.

Out of the methods stated above, efforts on boundary layer suction, boundary layer blowing, and vortex generator are found in literature accumulated by authors like Chang [5], Lachmann [6], Rosenhead [7], Goldstein [8], Schlichtingand [9] others.

But less effort was made on investigating the influence of Magnus Effect on the performance of aerofoil. [The Magnus effect is the commonly observed effect in which a spinning ball (or cylinder) curves away from its principal flight path] One of ways of this investigation is incorporating a rotating cylinder at the leading edge of aerofoil. By this, they tried to extract the advantages of Magnus effect and utilize it in increasing the performance of aerofoil. This way of research is under study for about last few decades.

Though the experimental works were conducted just after the invention of the concept but compilation of the research works and recording the experimental results started later on. Frequent investigations and experimental researches were carried out and outcome of those researches were recorded. To mention some of the recent researches in this area: from 1989 to 1998 several researches were done by Modi along with some other researchers to appreciate the effect of moving surfaces on the aerofoil boundary layer control [the concept of Boundary layer is invented by Prandtl and according to this concept the thin viscous region adjacent to the body is called boundary layer (10)] and increment of aerofoil performance [11-14]. In 2000, an experimental study was conducted on NACA 63218 by Al-Garni [15] along with some other researchers, simulation of which was conducted by Yahiaoui [16] along with some other researchers in 2015. An entire review of the researches conducted on Magnus effect was nicely compiled by Seifert [17] which served as a useful reference for the researchers of this field.

Application of this Magnus Effect on aircraft wing was studied by Patkunam [18]. He along with some other researchers proposed an approach called Flo-Lapse where they showed the way of incorporating Magnus effect on the wing of an aircraft and how it

increases the performance of that aircraft. They published their research on Oct-2015 [18].

Moreover, in the field of natural science, Kenyon [19] published his research in 2016, where he developed two algebraic formulae for calculation of Magnus force. Again, in the field of applied mechanics, Sailaranta [20] studied the influence of Magnus Effect on the flight of a fast spinning vehicle at high angle of attack. This research particularly focused on the consequences for the vehicle stability. The researcher also tried to investigate the possibilities to limit the terminal velocity and range of a bullet with the aid of Magnus effect. This research was also conducted in 2016. All these proves that, Magnus effect as a current research topic.

To continue the flow of this research, some avenues are found out according to the suggestion put forward by previous researches. Thus, establishing the performance curves of leading edge rotating cylinder at various rotating speed and comparing the results with simulation is required to confirm the influence of Magnus effect in practical applications. For doing that NACA 4 digit aerofoil is used because this is the most widely used aerofoil series.

CHAPTER 3

EXPERIMENTAL SETUP

3.1 Basic Setup

3.1.1 Subsonic Wind Tunnel (Model AF100)

3.1.1.1 Description

In this investigation an open circuit subsonic wind tunnel (Model AF 100 of TQ Equipment, U.K.) with a working section of 300 mm by 300 mm and 600 mm long is used as shown in Figure 3.1. It is a compact, open-circuit, suction wind tunnel for studying aerodynamics. The subsonic wind tunnel saves time and money compared with full-scale wind tunnels and it offers a wide variety of experiments. The subsonic wind tunnel gives accurate results and is suitable for general study and research projects.

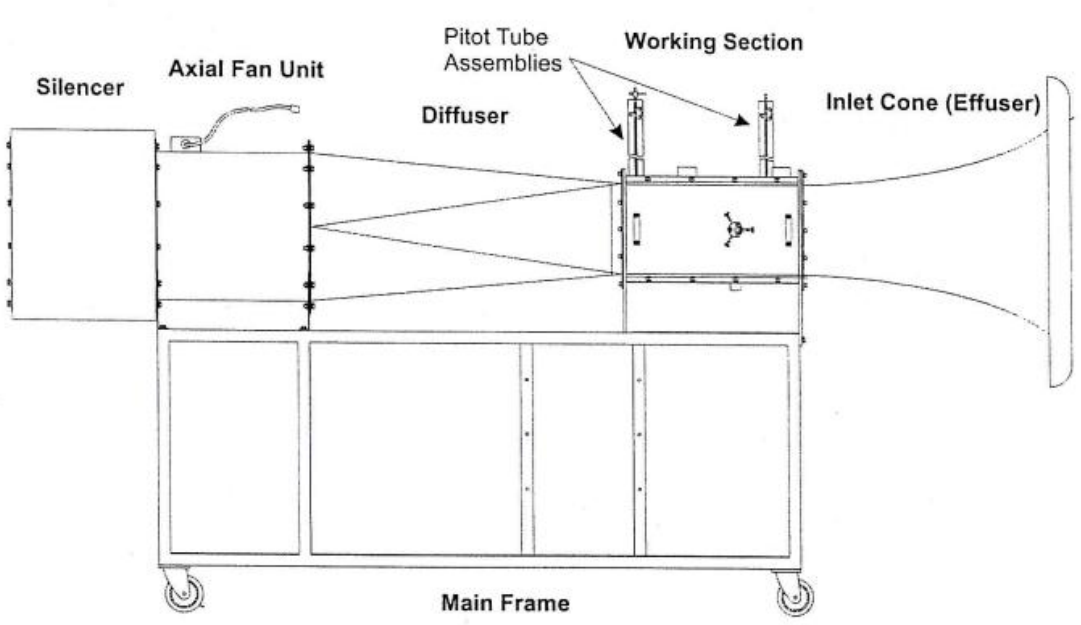

Figure 3. 1 AF 100 General Layout

3.1.1.2 Features

- Saves time and money compared to full-scale wind-tunnels or airborne laboratories
- Operates at meaningful Reynolds numbers
- Compact, open-circuit suction design
- Wide variety of experiments in aerodynamics
- Comprehensive selection of optional instrumentation, models and ancillaries
- High levels of safety
- Controls and instrumentation conveniently mount on a separate, free standing frame
- Works with TecQuipment's Versatile Data Acquisition System (VDAS) to allow accurate real-time data capture, monitoring and display on a computer

3.1.1.3 Operation

Air enters the tunnel through an aerodynamically designed effuser (cone) that accelerates the air linearly. It then enters the working section and passes through a grill before moving through a diffuser and then to a variable-speed axial fan. The grill protects the fan from damage by loose objects. The air leaves the fan, passes through a silencer unit and then discharges back into the atmosphere. A separate control and instrumentation unit controls the speed of the axial fan (and the air velocity in the working section). The control and instrumentation unit also includes manometers and electrical outlets to supply electrical power to other optional instruments.

3.1.2 Three-Component Balance (Model AFA3)

Measures lift, drag and pitching moment of models in TecQuipment's Subsonic Wind Tunnel

3.1.2.1 Description

The Three-Component Balance fits onto the working section of Subsonic Wind Tunnel (AF100). It offers an easy-to-use support system for wind tunnel models. It measures lift, drag and pitching moment exerted on the model. The balance attaches to the vertical wall of the wind tunnel working section. It is designed for air flows from right to left when the balance is viewed from the front. The balance comprises a mounting plate

secured to the wind tunnel working section. A triangular force plate is held on the mounting plate by a mechanism that constrains it to move in a plane parallel to the mounting plate only, while leaving it free to rotate about a horizontal axis. This arrangement provides the necessary three degrees of freedom. The forces acting on the model are transmitted by cables to three strain gauged load cells. The output from each load cell is taken via an amplifier to a microprocessor-controlled display module. The display module mounts onto the wind tunnel control and instrumentation frame and includes a digital display to show the lift, drag and pitching moment directly. The equipment is fully compatible with TecQuipment's Versatile Data Acquisition System (VDAS). Using VDAS enables accurate real-time data capture, monitoring, display, calculation and charting of all relevant parameters on a suitable computer. The model support of the balance can be rotated by 360 degrees. This allows adjustment of the angle of incidence of the model to the direction of air flow. The model support is locked in the required position by a simple clamp after adjustment. The Angle Feedback Unit fits onto the Three-Component Balance and transmits the rotational angle of the test model back to the automatic data acquisition unit.

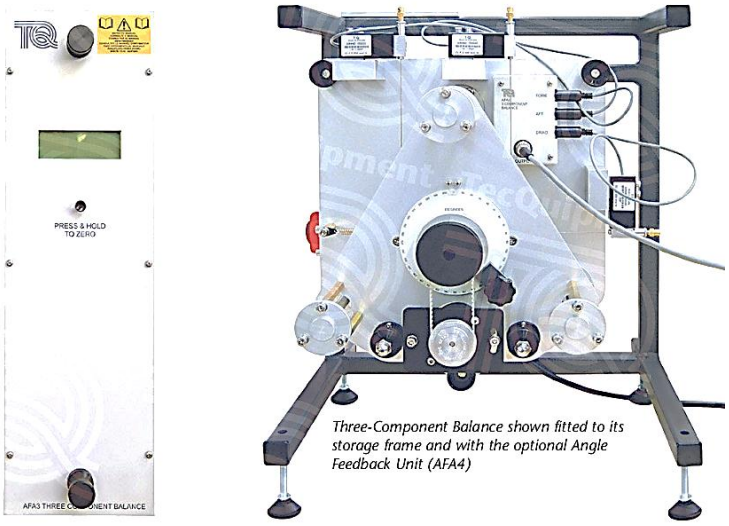

Figure 3. 2 Three-Component Balance (Model AFA3)

3.1.2.2 Features

- Provides a convenient support system for models to measure the lift, drag and pitching moment.
- Fully compatible with Versatile Data Acquisition System (VDAS) to enable accurate real-time data capture, monitoring and display on a computer.

- Digital display shows lift, drag and pitching moment directly.
- Allows full adjustment of angle of incidence of the model to direction of air flow.

3.1.3 Balance Angle Feedback Unit (Model AFA4)

Measures angular positions of models mounted on TecQuipment's Three-Component Balance (Model AFA3) with the Versatile Data Acquisition System

3.1.3.1 Description

The Balance Angle Feedback Unit is used to measure the angular position of models mounted on the balance in Subsonic Wind Tunnel (Model AF100). The Angle Feedback Unit mounts on the Three-Component Balance attached to the wind tunnel. It then transmits the rotational angle of the model to Versatile Data Acquisition System. The angle of the model can then be logged on a suitable computer along with other captured experimental data.

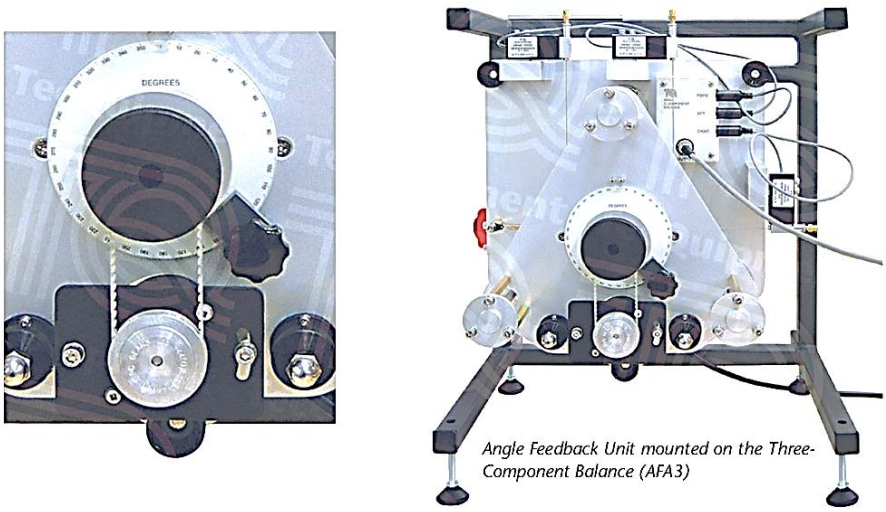

Figure 3. 3 Balance Angle Feedback Unit (Model AFA4)

3.1.3.2 Features

- Provides a convenient means of measuring angles.
- Fully compatible with Versatile Data Acquisition System (VDAS).
- Digital display shows angular measurements.

3.1.4 Differential Pressure Transducer (Model AFA5)

Microprocessor-controlled pressure measurement and display unit for use with Subsonic Wind Tunnel.

3.1.4.1 Description

It measures and displays pressures in Pitot-static tubes and other pressure-sensing devices fitted to a wind tunnel, with respect to the atmosphere or differential pressures. The control and instrumentation panel of the AF100 wind tunnel includes a location for mounting up to two Differential Pressure Transducer modules. It is microprocessor-controlled and contains a calibrated pressure transducer. The unit has an integral liquid crystal display that allows the user to read pressure directly. The signals of the pressure sensors may be shown as output to Versatile Data Acquisition System (VDAS). Using VDAS enables accurate real-time data capture, monitoring, display, calculation and charting of all relevant parameters on a suitable computer. When the Differential Pressure Transducer is used with the automatic data acquisition unit it provides a significant advantage over conventional instruments such as manometers.

Figure 3. 4 Differential Pressure Transducer (Model AFA5)

3.1.4.2 Features

- Measures and displays differential pressures from models, Pitot static tubes and other devices
- Quicker, easier and more versatile than using liquid manometers
- Integral LCD allows direct pressure measurement
- Measures differential pressures or pressure with respect to atmosphere
- Fully compatible with TecQuipment's Versatile Data Acquisition System (VDAS) to enable accurate real-time data capture, monitoring and display on a computer

3.1.5 Pitot-Static Traverse (300 mm) (Model AFA7)

A traversing Pitot-static tube with electronic position measurement for use with Subsonic Wind Tunnel (Model AF100).

3.1.5.1 Description

It is a Pitot-static tube that mounts in the working section of the wind tunnel, either upstream or downstream of the position of the test model. The vertical position of the tube, which is adjustable, is displayed on a digital indicator. The digital indicator position can be set to zero in any position. This allows the datum or starting point of an experiment to be defined by the user. To display differential pressure, the Pitot-static tube connects to a manometer supplied with the wind tunnel.

The pressure signals from the Pitot-Static Traverse (as shown in Figure 3.5) may be shown as output to Versatile Data Acquisition System (VDAS) to allow computerized data acquisition and display. For pressure measurement this will require the optional Differential Pressure Transducer module (Model AFA5).

Figure 3. 5 Pitot-Static Traverse (300 mm) (Model AFA7)

3.1.5.2 Features

- Accurate digital display of position
- Zero facility allows the starting point of an experiment to be set in any position
- Works with TecQuipment's Versatile Data Acquisition System (VDAS) to give accurate real-time data capture, monitoring, and display on a computer

3.1.6 VDAS (Versatile Data Acquisition System)

Versatile Data Acquisition System (as shown in Figure 3.6) enables high-capacity, accurate, efficient and user-friendly digital automatic data acquisition.

3.1.6.1 Description

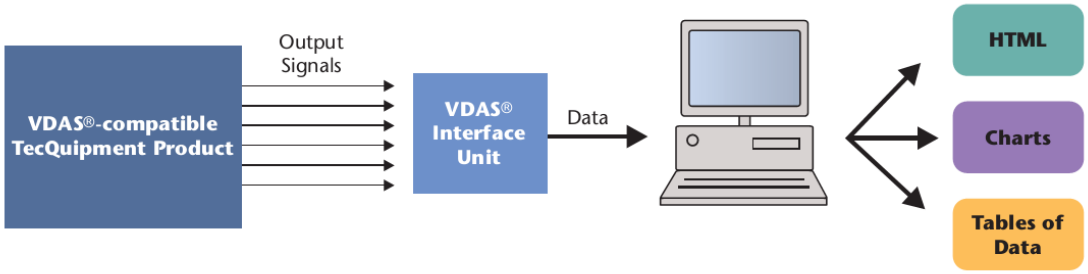

Figure 3. 6 Schematic diagram of Versatile Data Acquisition System

The system consists of software which is intuitive and easy to use, with clear and convenient data display options. This saves a lot of time by giving processed data.

Figure 3. 7 Versatile Data Acquisition System

3.1.6.2 Features

- Modern, cost-effective digital automatic data acquisition hardware, software and accessories to enhance teaching and laboratory sessions.
- Highly versatile system for use with equipment from many TecQuipment product ranges.
- Enables real-time data capture, monitoring and display of all relevant parameters on a computer (PC).
- Highly accurate and noise-resistant.
- Software is intuitive and easy to use, with clear and convenient data display options.
- Fast and convenient automatic calculation, recording, charting and export of relevant data and parameters make efficient use of time.

3.1.6.3 Technical Characteristics

The software has a comprehensive range of functions, including:

- Recording data automatically or with some manual input
- Display of real-time data, either in digital form or as an analogue meter
- Logging data for printing and later analysis
- Exporting data for use by other software
- Performing real-time calculations to generate user-defined data
- Creating and printing charts and data tables

In addition, the high flexibility of the software enables users to create, save and reuse their own custom layouts if required.

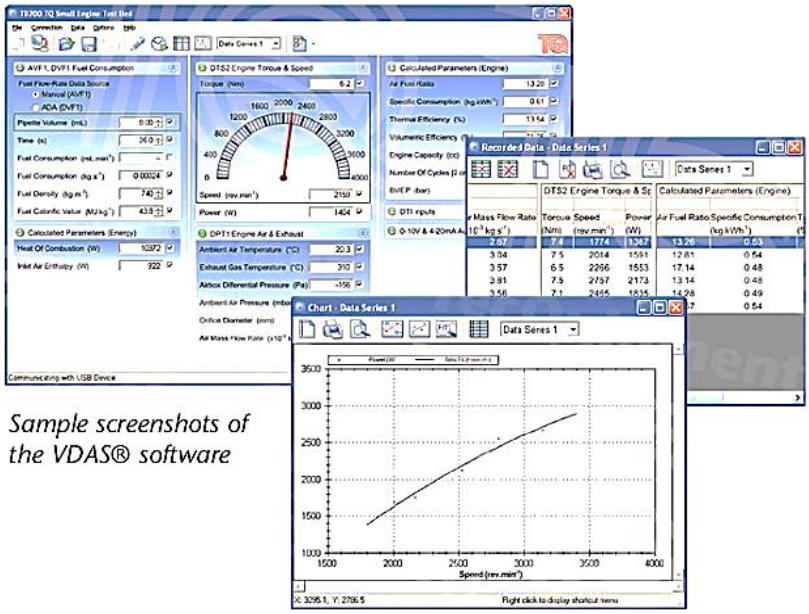

Figure 3. 8 Screenshots of VDAS software

3.2 Procedure of Calibration of Three Component Balance

Before starting the measurement the wind tunnel performance was tested several times with manufacturer's supplied aerofoil associated data. Initially as it was to give some data which varied from the supplied one. It was decided to calibrate the three component balance. It was then checked with the given procedure supplied by the manufacturer. Detailed is described below:

Before doing Calibration of Three Component Balance, the following were done:

1) The balance was fitted to its calibration/storage frame and the assembly was placed onto to a table so that the back of the apparatus was close to the edge of the table.
2) The large pulley wheel was turned around to the rear of the frame.
3) The cable was connected from the balance to the display unit.
4) A spirit level was used across the top of the back plate to make sure that the balance was level, adjust the four feet of the calibration frame if necessary. Also, the spirit level was placed above the back of the back plate to check that it was vertical.

5) The ‘T’ shaped calibration arm was slide from the top of the calibration frame and was inserted into the model holder from behind, with the bar roughly horizontal.
6) On the display module, the ‘zero’ button was pressed and hold while at the same time, the power was switched on. It took a few seconds for the unit to settle. The display was in the calibration mode which showed the individual readings from the load cells as ‘FORE’, ‘AFT’ and ‘DRAG’ (the display normally shows lift, drag and pitching moment).
7) The centering clamps were released. The zero readings for each of the load cell should be 0 +/-5 N. A note of the entire zero’ readings was made.

Now, the following procedures were followed to do the calibration:

3.2.1 Calibration Procedure of Drag Cell

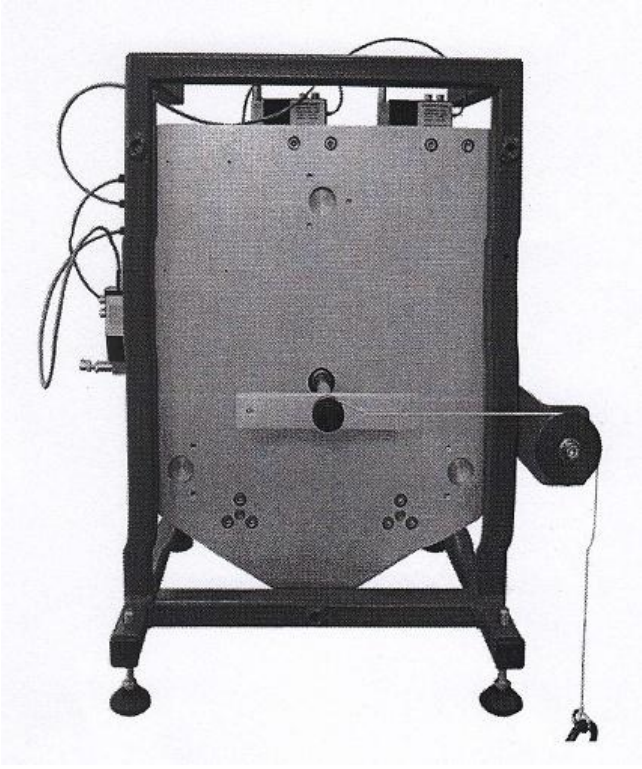

Figure 3. 9 Calibration Checking Procedure of Drag

In order to do the calibration the following steps were carried out:

1) The small pulley was unscrewed and fitted to the central hole on the calibration arm.
2) The looped end of the cord (supplied) around the small pulley was fitted.
3) The cord was run around the large pulley.
4) A range of masses starting from 0 kg to 5 kg mass from the ringed end of the cord were hung and the corresponding drag cell values were record.
5) DRAG cell value was read; the zero reading was subtracted.
6) A graph for final DRAG cell values Vs actual weight was drawn.
7) The graph resulted in a straight line going through the origin and thus the drag cell was in good condition

DRAG Cell Calibration Data

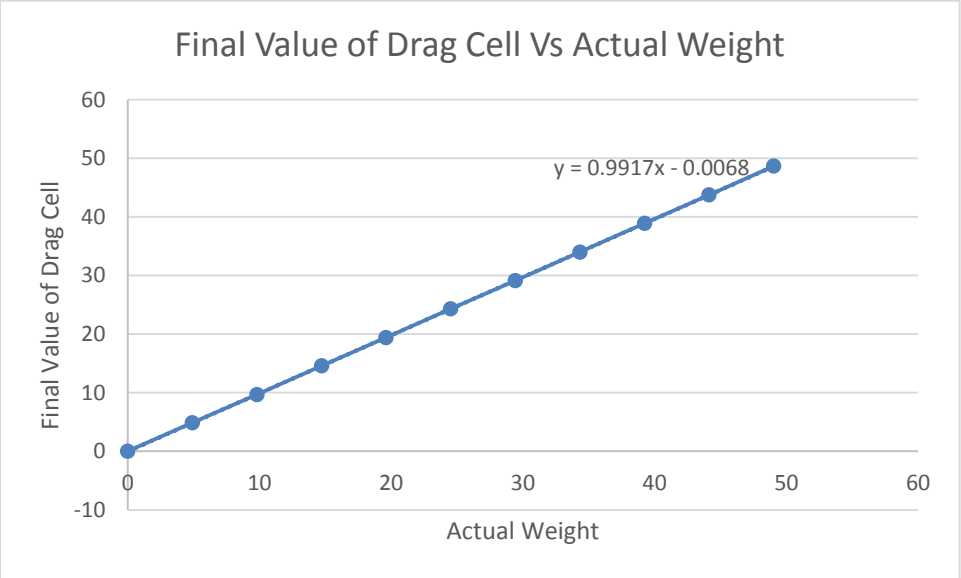

Figure 3. 10 Final DRAG cell values Vs Actual Weight

3.2.2 Calibration Procedure of FORE & AFT Cell

In order to do the calibration the following steps were carried out:

1) The mechanical wire coming out from the FORE load cell was allowed to hang straight down.
2) A range of masses starting from 0 to 5 kg with an increment of 0.5 kg were attached and corresponding FORE cell values were recorded.
3) The zero reading was subtracted and final FORE cell values were recorded.
4) A graph between final values of FORE cell Vs Actual Weight was draw and the graph resulted in a straight line.
5) The graph resulted in a straight line and the final FORE cell value was recorded when the actual weight was 0 N
6) Steps 1 to 5 for AFT cell were repeated.
7) The magnitudes obtained from FORE and AFT load cells were added and recorded
8) The force plate was weighed.
9) The value obtained from step 7 was equal to the value obtained from step 8 and thus the cells were ok.

FORE & AFT Cell Calibration Data:

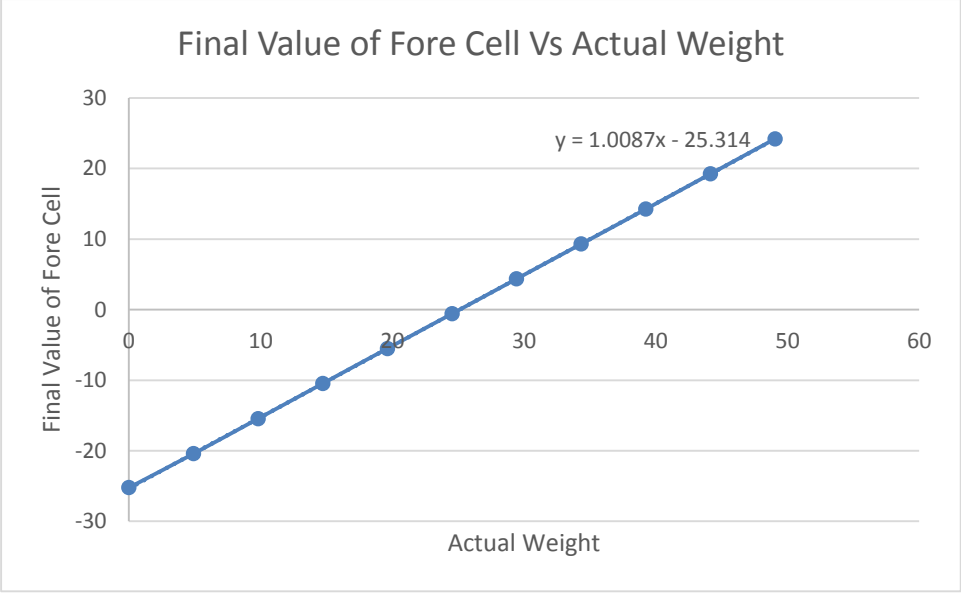

Figure 3. 11 Final Values of FORE cell Vs Actual Weight

Magnitude of final FORE cell when actual weight is zero = 25.23 N

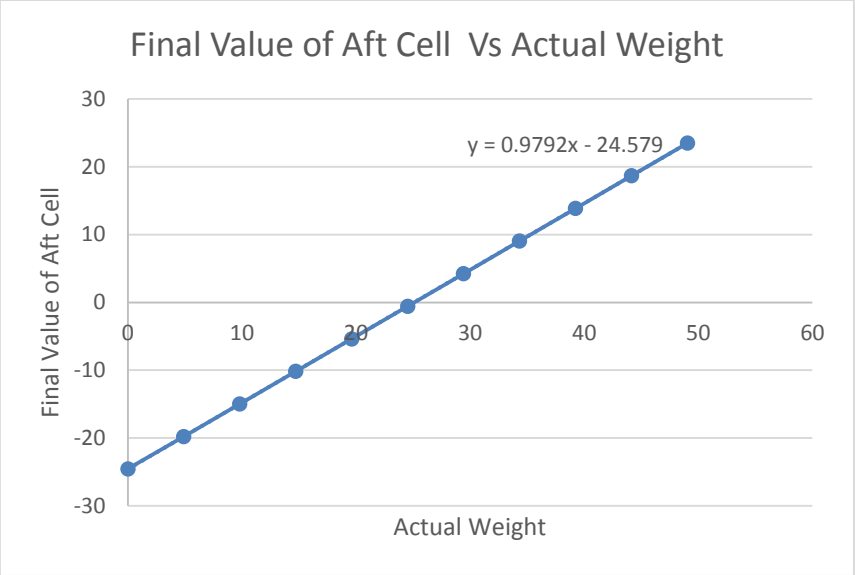

Figure 3. 12 Final AFT Cell Values Vs Actual Weight

Magnitude of final AFT cell when actual weight is zero = 24.54 N

Total magnitude from FORE & AFT cell = 25.23 + 24.54 = 49.77 N

Mass of the force plate = 5 kg

Weight of the force plate = 5 X 9.81 = 49.05 N

% of error = [(49.77-49.05)/49.05] X 100 = 1.46% which is negligible.

3.3 Wind Tunnel Calibration Validation

For the sake of validation of the calibration activities, factory provided ideal data of NACA 2412 were considered and same values were taken with the calibrated wind tunnel. These are presented below:

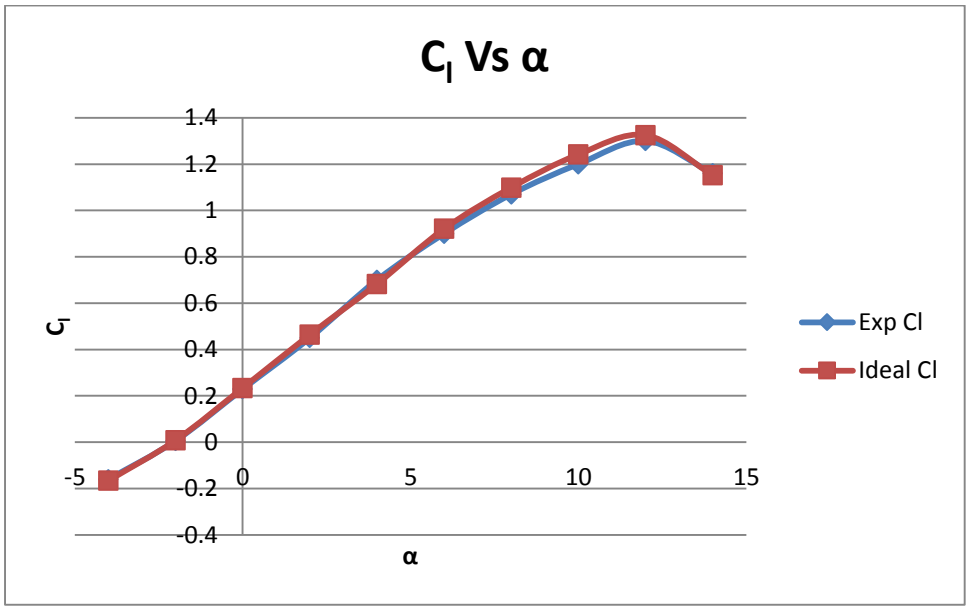

Figure 3. 13 Experimental Vs Ideal Values of Cl

Figure 3.13 shows the comparison of lift coefficient between experimental data and ideal data provided by the manufacturer where both of them have a strong agreement up to angle 7 degree. After that experimental data deviates a little from the ideal data but again they stalled at the same angle and agreed again for the following angles.

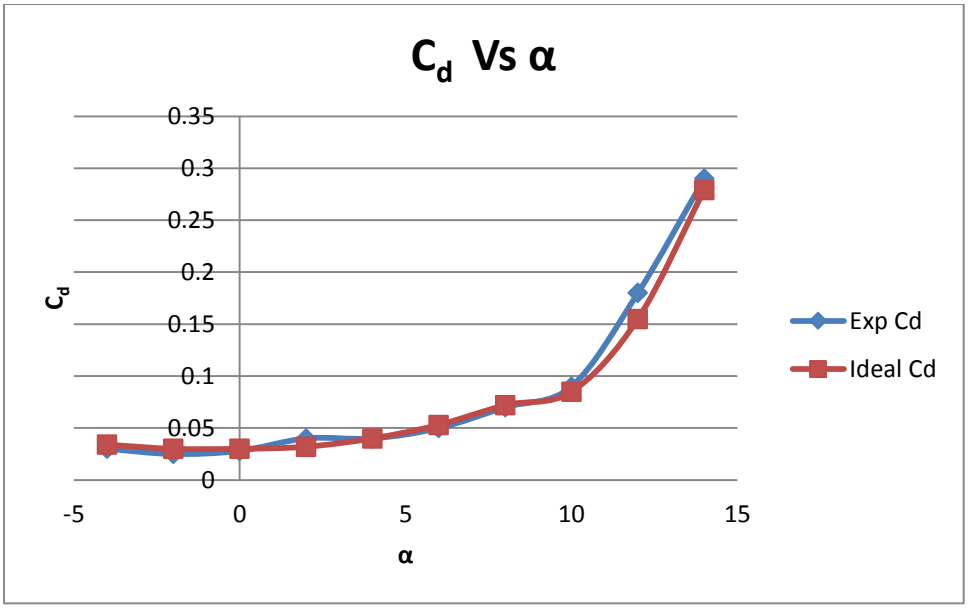

Figure 3. 14 Experimental Vs Ideal Values of Cd

Figure 3.14 illustrates the comparative drag coefficient curve between the experimental and ideal data where the values agrees strongly up to angle 10 degree with an exception at 2 degree angle of attack where the experimental value obtained was little higher than the ideal one. After 10 degree angle of attack, experimental values are little higher than the ideal value and it continues up to 14 degree angle of attack.

3.4 Modifications Done to Existing Side walls of Working Section

Both front and back side walls were modified by creating a groove in them. Grooves were created in the wall in order to allow the movement of the rotating cylinder at the leading edge of the aerofoil at different angles of attack.

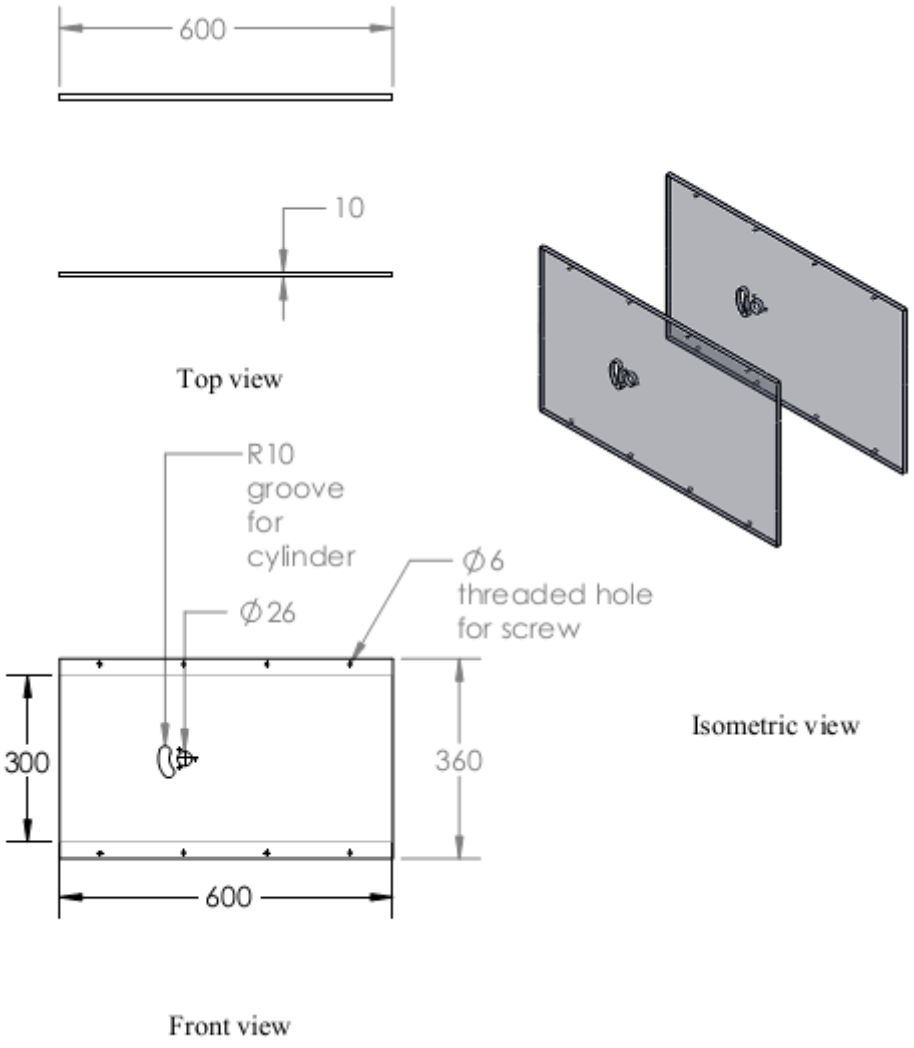

Figure 3. 15 Modified Side walls [all dimensions are in mm]

3.5 Experimental Setup

3.5.1 NACA 0018 Aerofoil

As symmetric aerofoil, NACA 0018 was selected whose chord is 150 mm and span 300 mm.

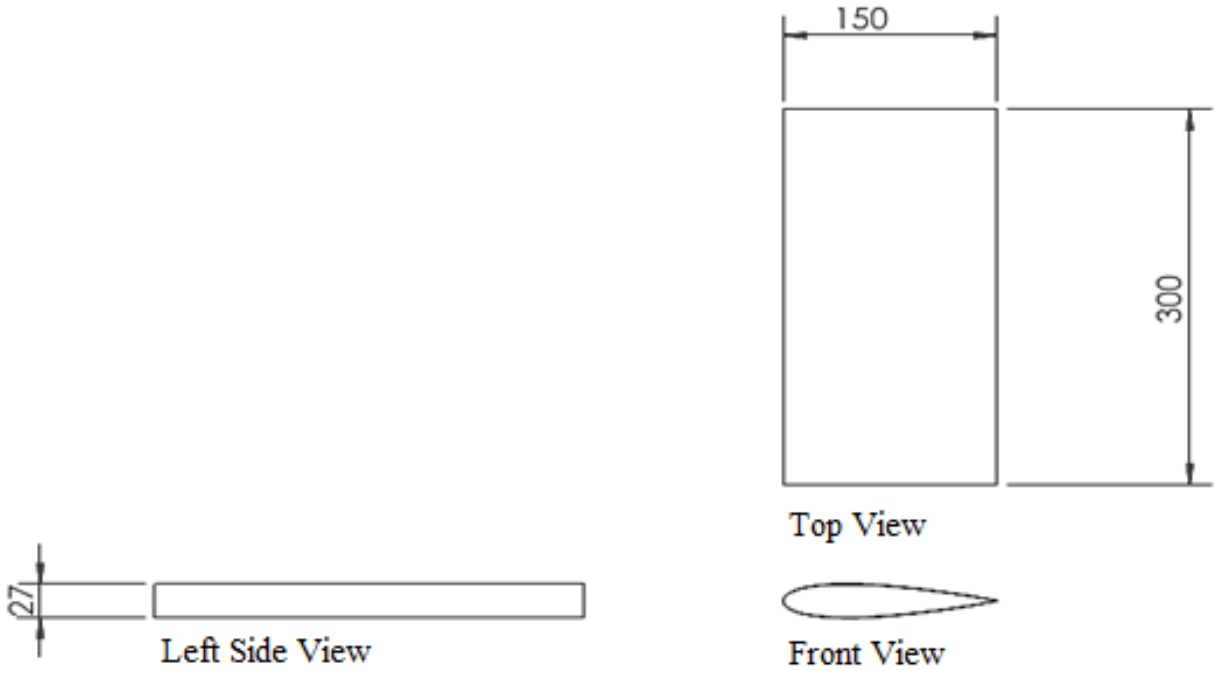

Figure 3. 16 NACA 0018 aerofoil [all dimensions are in mm]

3.5.2 NACA 0018 Aerofoil with groove

NACA 0018 with a groove of 9 mm radius which facilitated the cylinder to be placed at the leading edge.

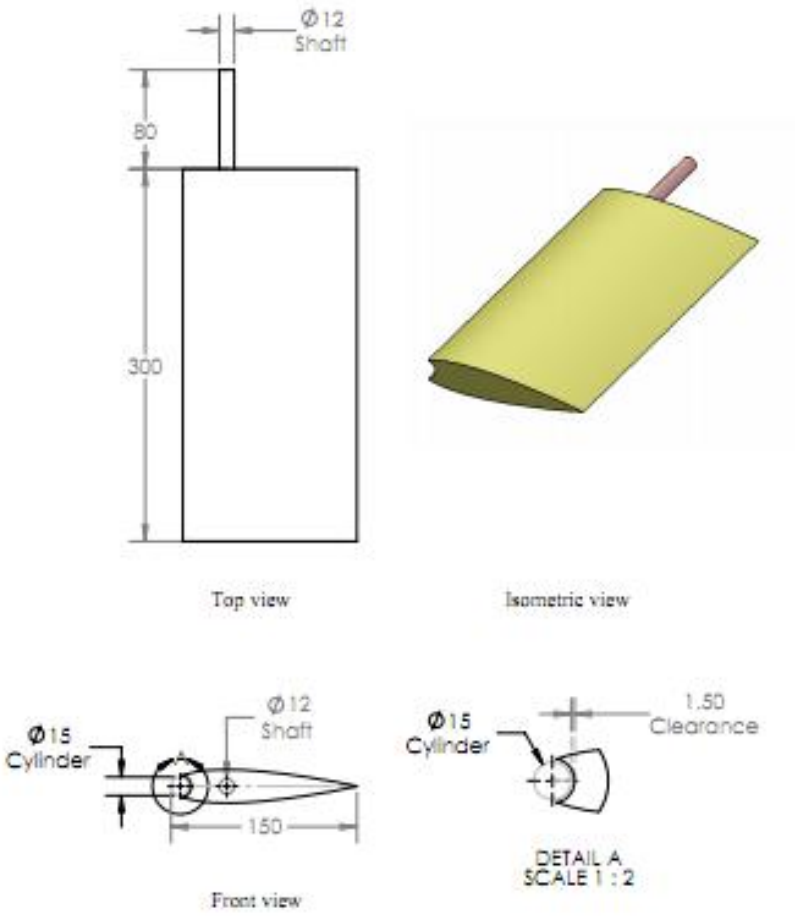

Figure 3. 17 NACA 0018 with groove [all dimensions are in mm]

3.5.3 Cylinder

A cylinder (made of wood) of 15 mm was chosen to be placed at the leading edge of the aerofoil.

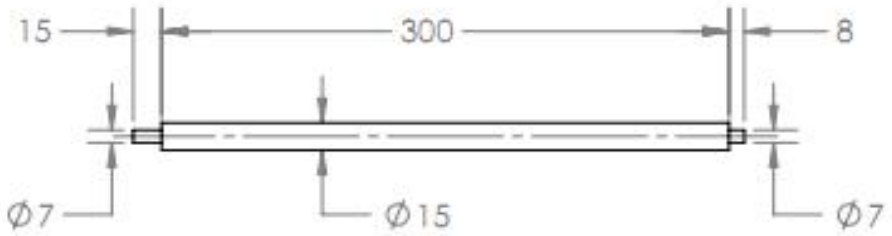

Right view

Isometric view

Figure 3. 18 Cylinder [all dimensions are in mm]

3.5.4 NACA 0018 Aerofoil with cylinder at the leading edge

NACA 0018 with the cylinder at the leading edge

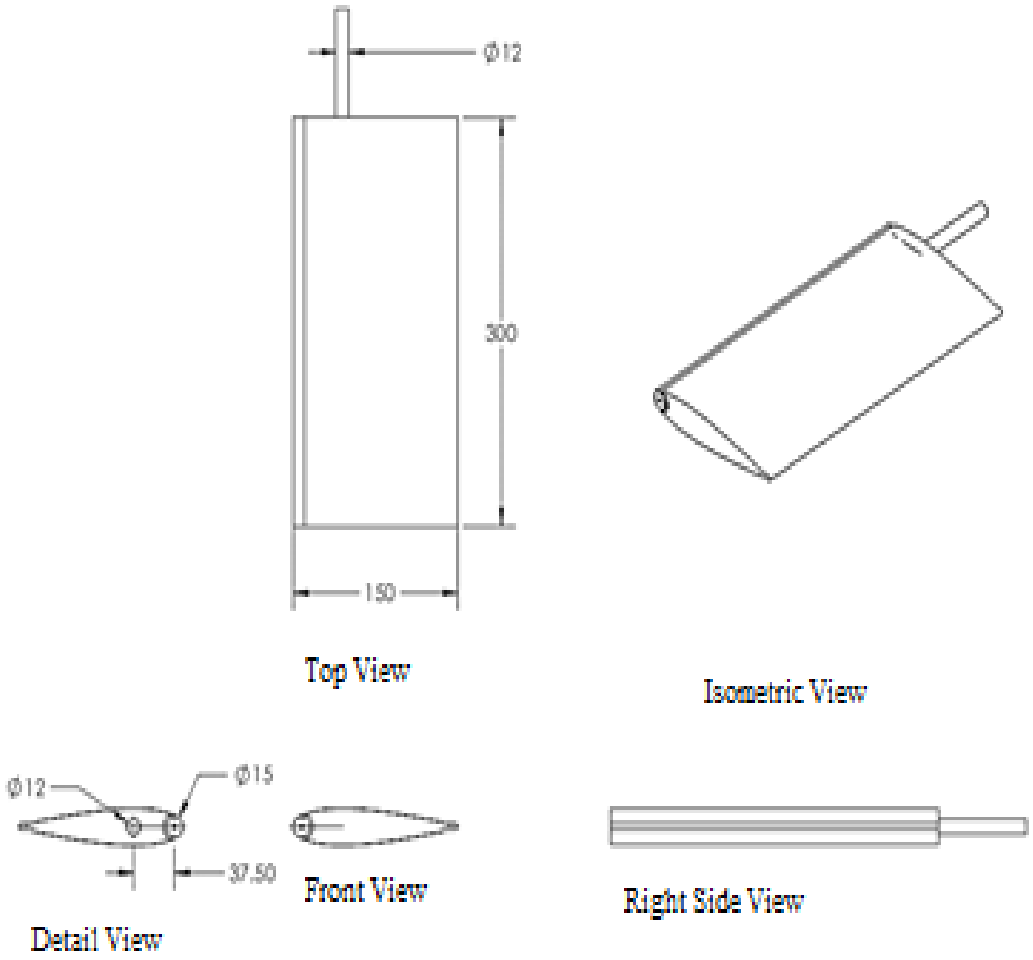

Figure 3. 19 NACA 0018 with cylinder at leading edge [all dimensions are in mm]

3.5.5 Coupler

A coupler was designed in order to connect the cylinder with the motor

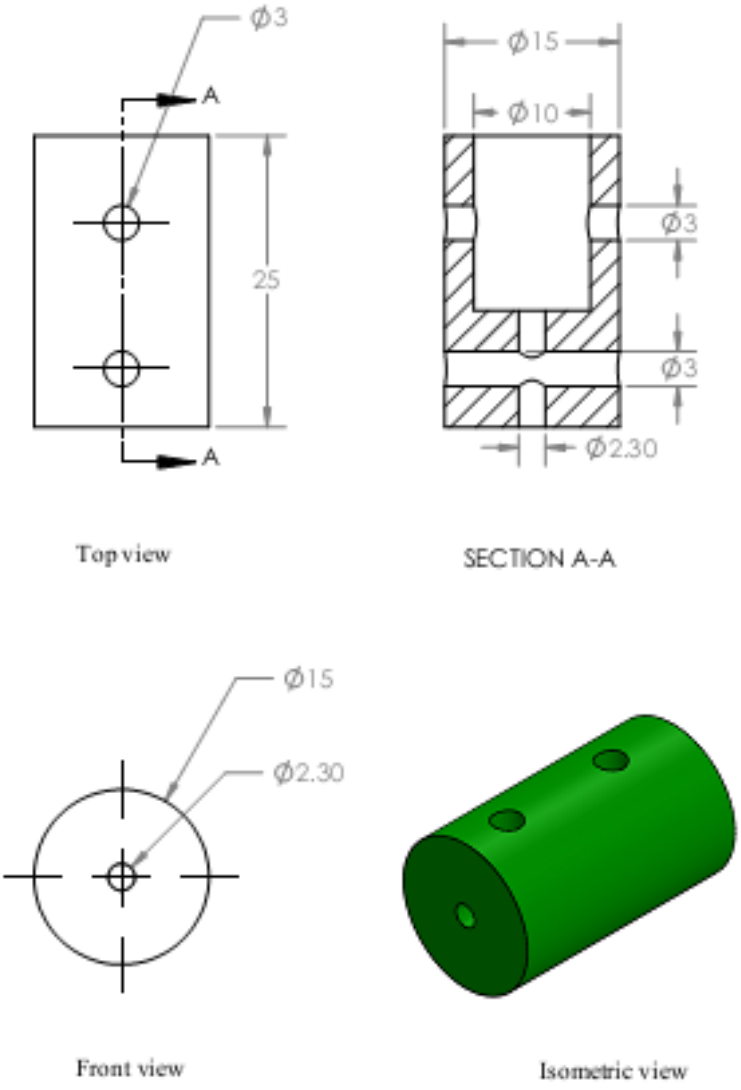

Figure 3. 20 Coupler [all dimensions are in mm]

3.5.6 Motor

A motor was used to rotate the cylinder placed at the leading edge of aerofoil

3.5.7 Motor with Cap

Selected motor with cap

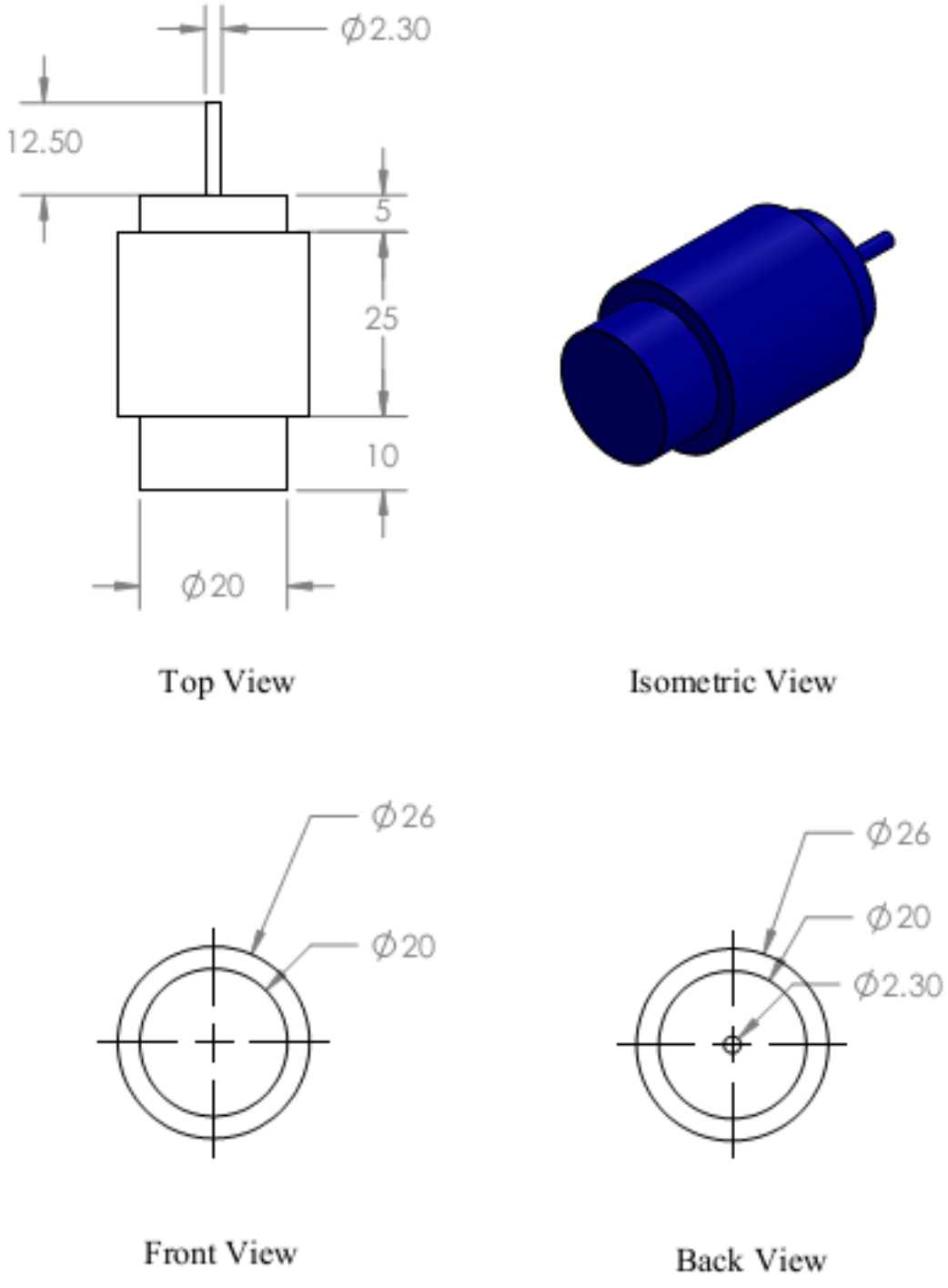

Figure 3. 21 Motor with cap [all dimensions are in mm]

3.5.8 Front Belt

It was used to connect the front disc with the motor. It was used in order to facilitate the cylinder as well as the aerofoil to rotate about same center

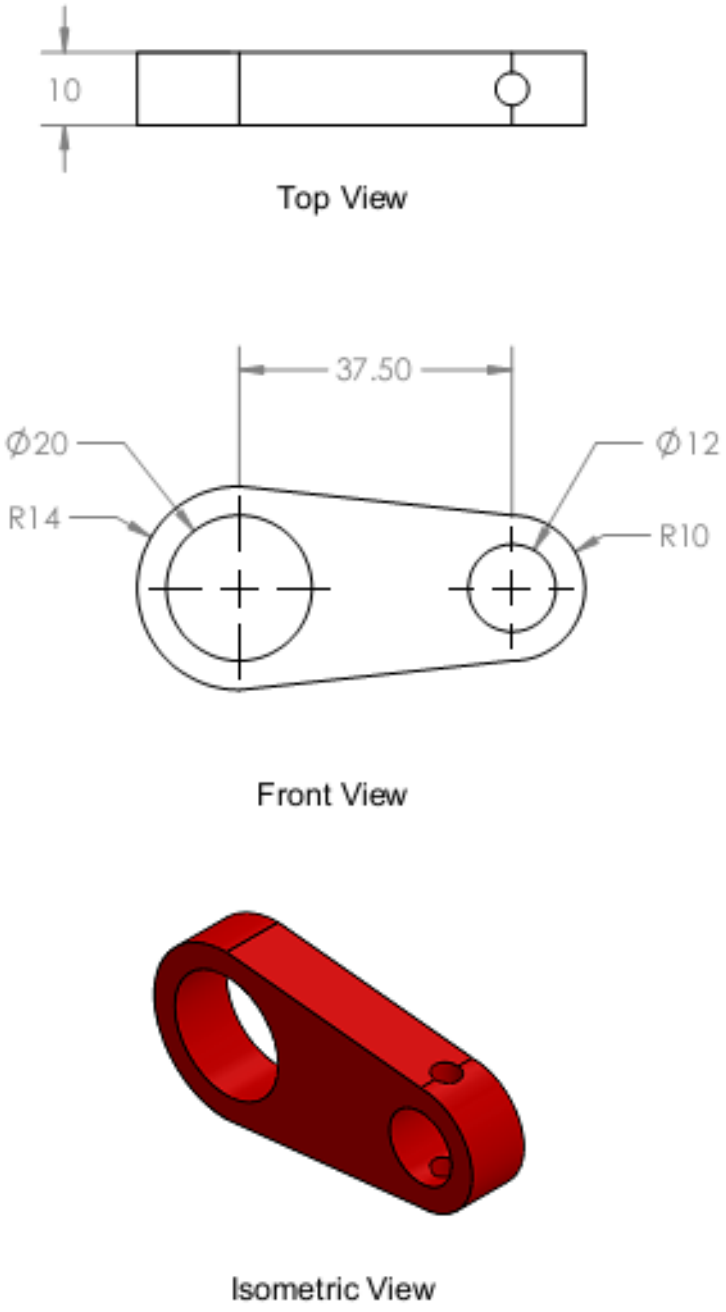

Figure 3. 22 Front belt [all dimensions are in mm]

3.5.9 Disc at front wall

This disc was designed to hold the motor through front belt

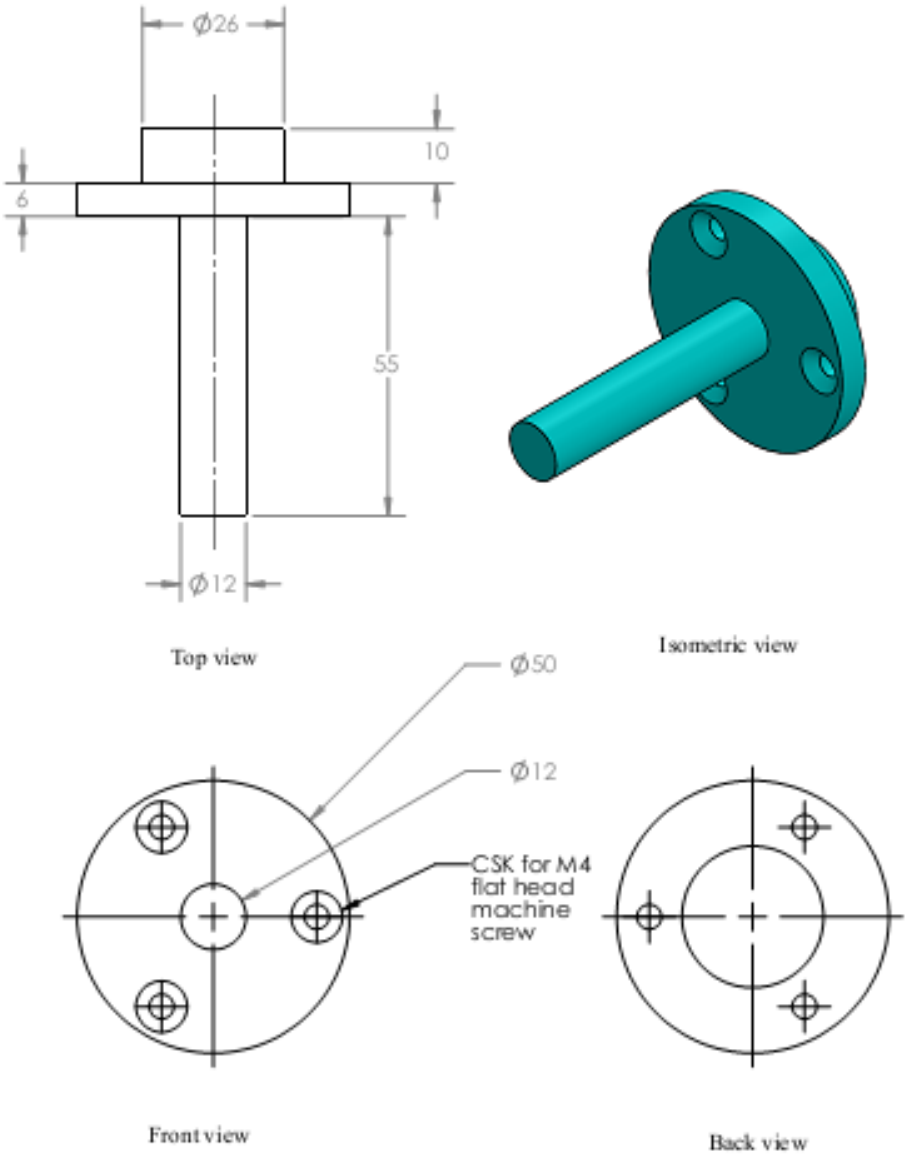

Figure 3. 23 Disc at front wall [all dimensions are in mm]

3.5.10 Disc at rear wall

On this disc the rear belt was fitted.

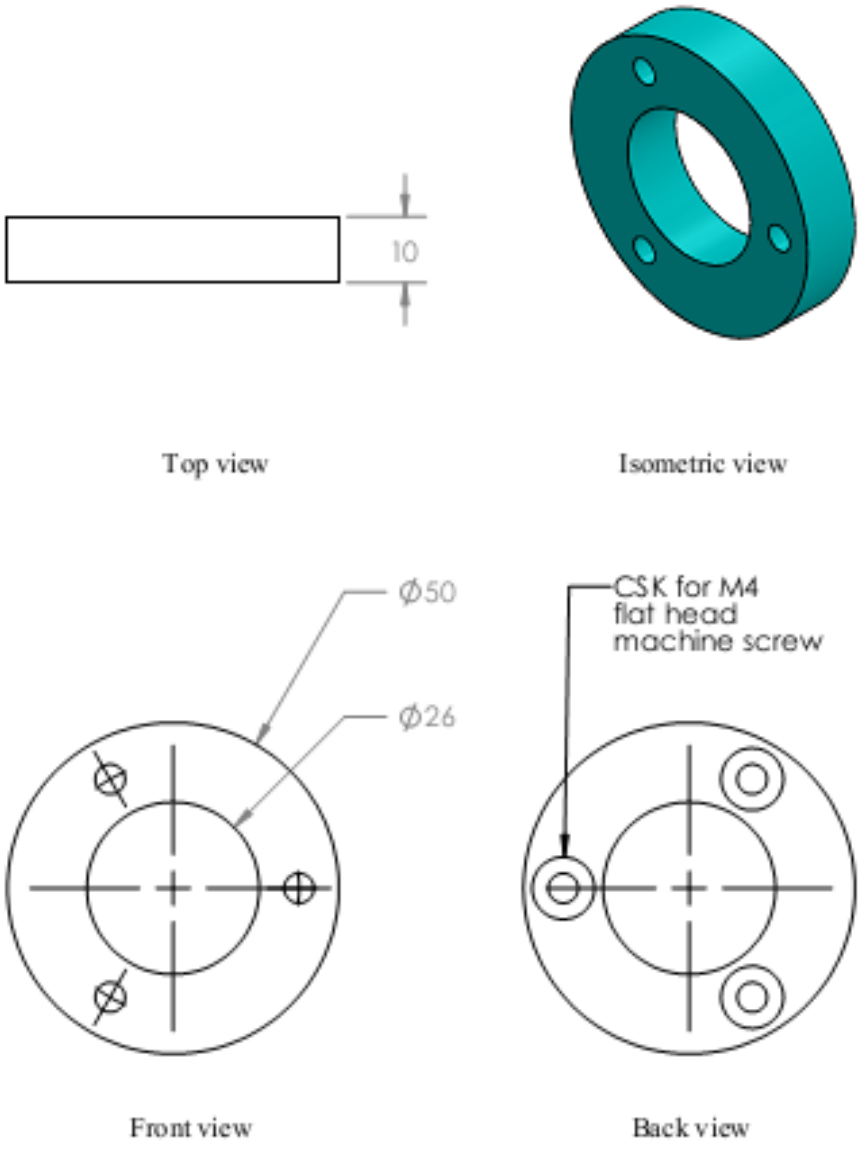

Figure 3. 24 Disc at rear wall [all dimensions are in mm]

3.5.11 Rear Belt

It was used to hold the rear portion of the cylinder placed at leading edge of the aerofoil

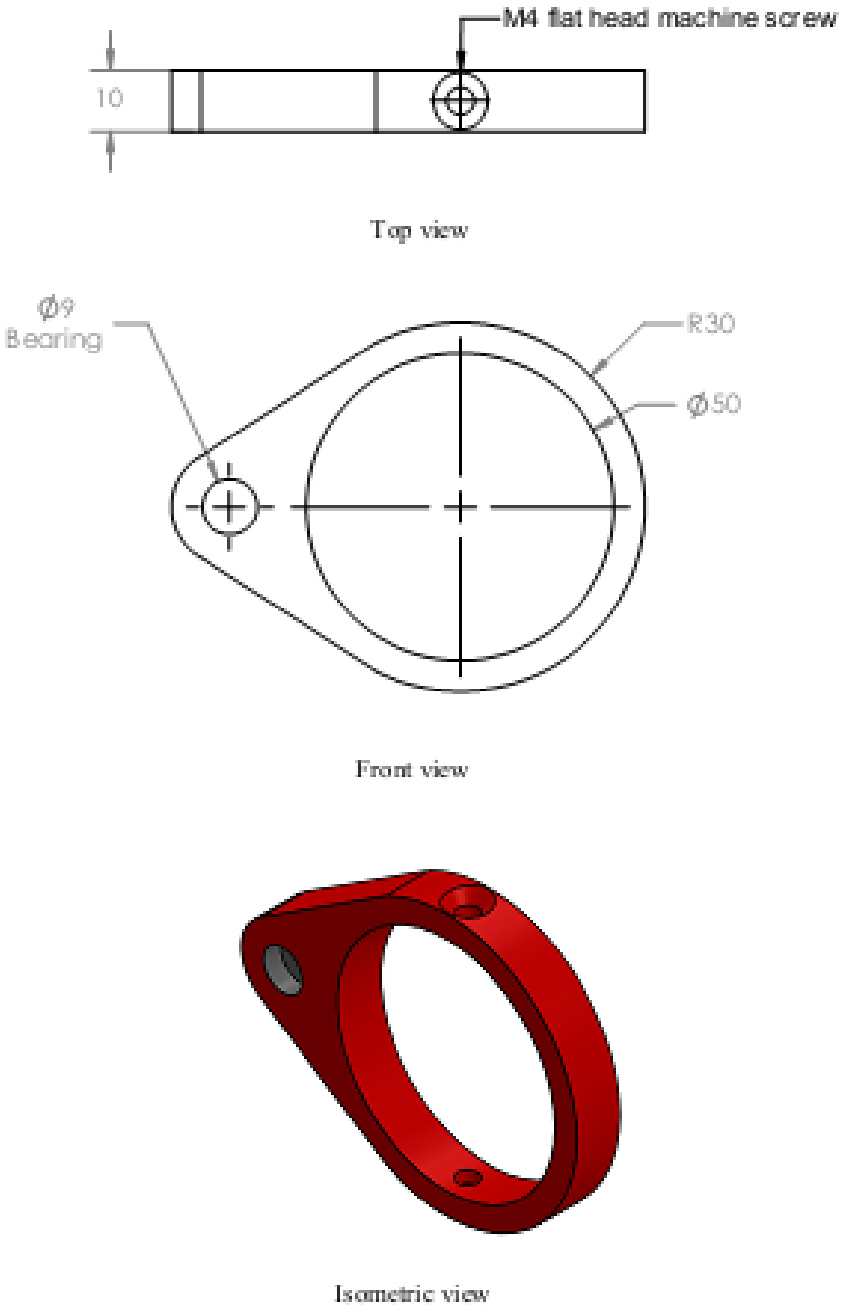

Figure 3. 25 Rear belt [all dimensions are in mm]

3.5.12 Cylinder Cap

The cylinder cap was used to connect the cylinder with the bearing.

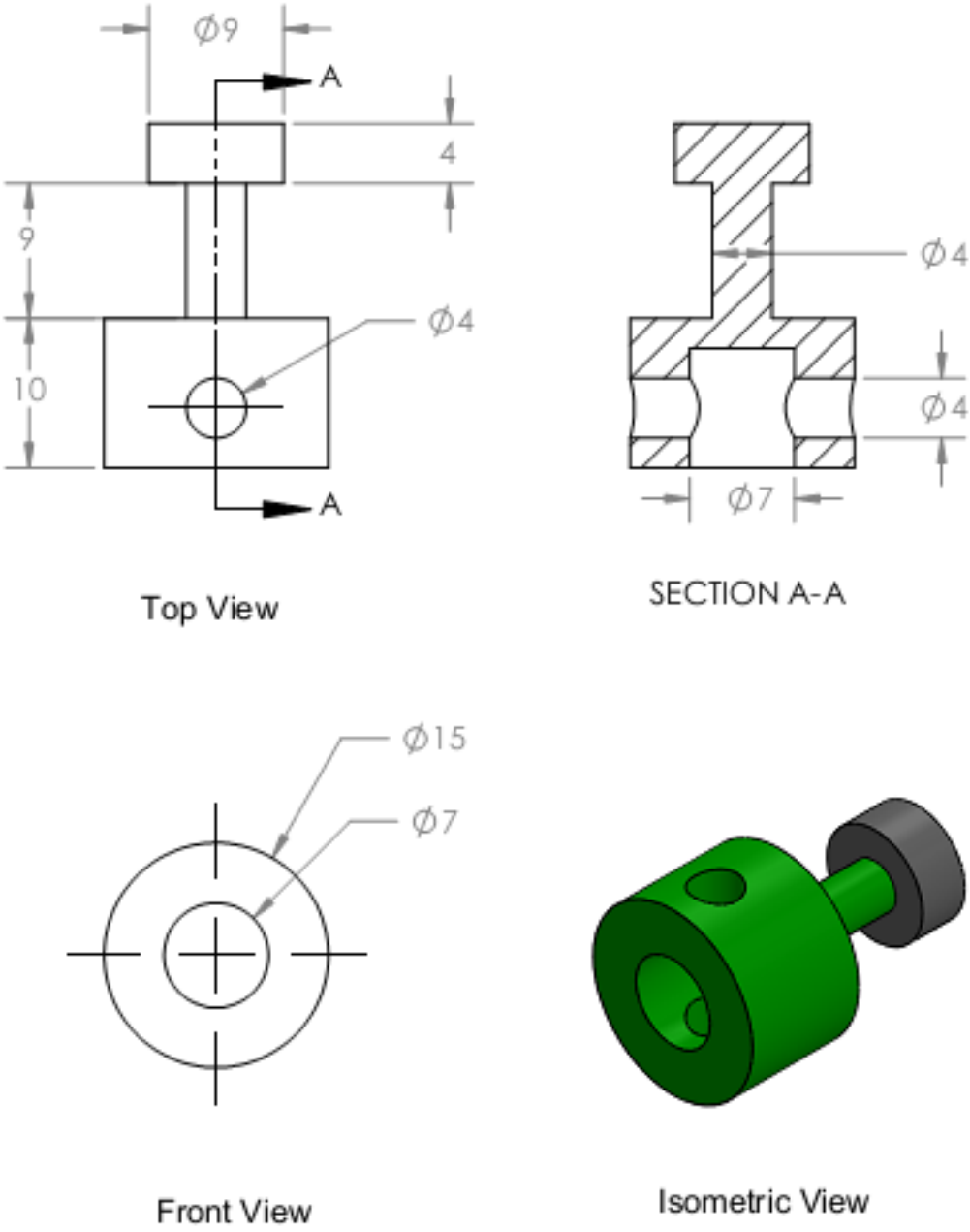

Figure 3. 26 Cylinder Cap

3.5.13 Final Assembly

Finally the modified test section looks like this

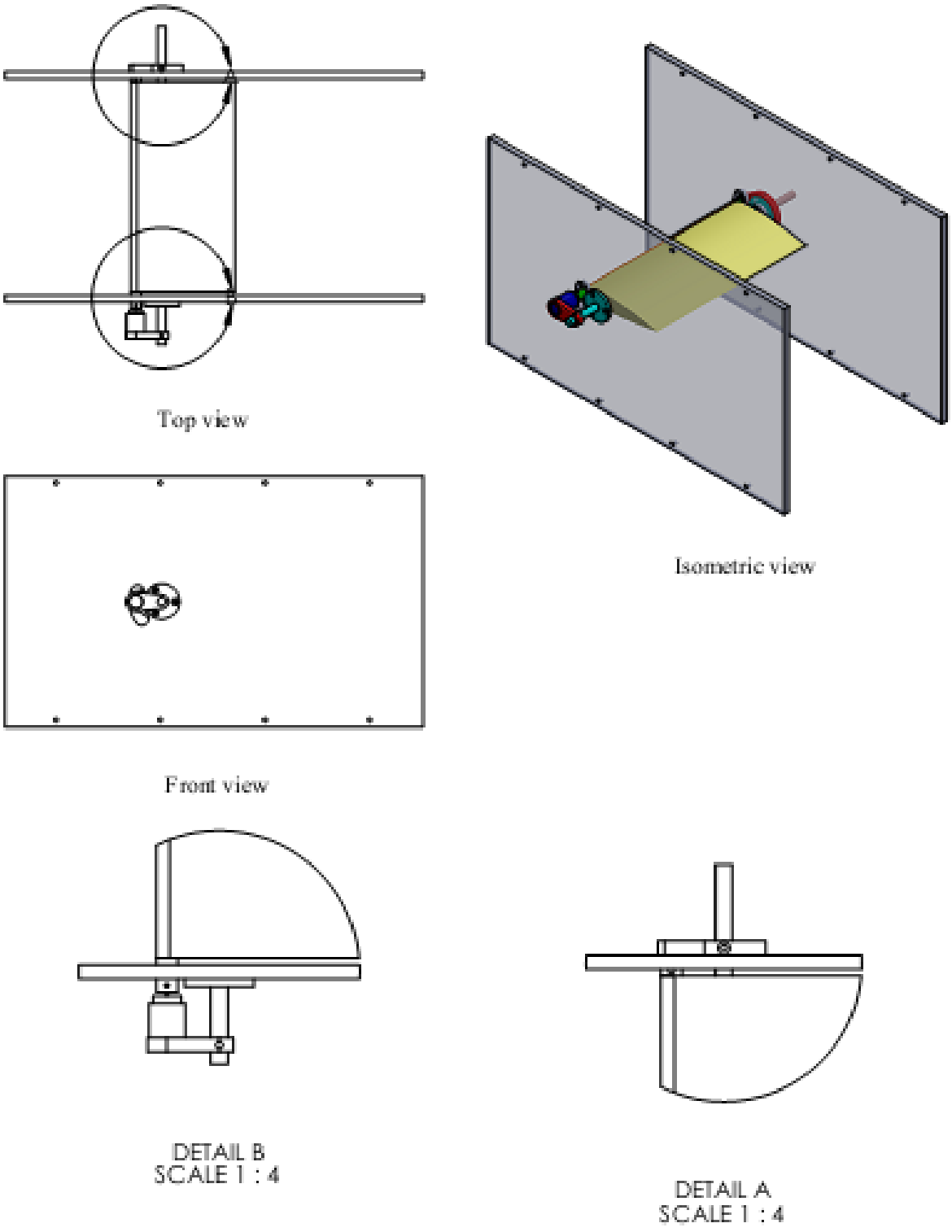

Figure 3. 27 Final Assembly [all dimensions are in mm]

CHAPTER 4

RESULTS AND DISCUSSIONS

4.1 TURBULENCE MODEL VALIDATION

In the present investigation simulations were performed in ANSYS. For calculation, the flow field around the aerofoil was taken from 6.5 chord length ahead of it and spread up to 17 chord length downstream and along the transverse direction the field spread to 7 chord length above and below the aerofoil as shown in the Figure 4.1 is divided into 152447 cells.

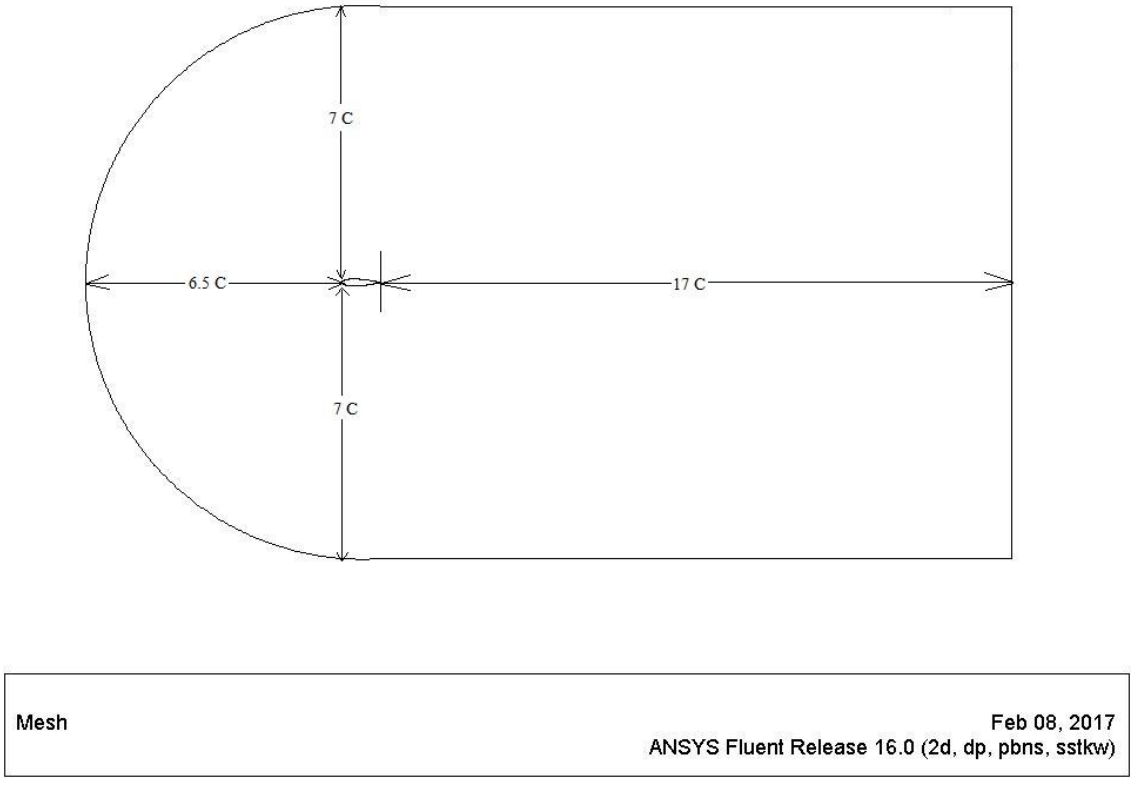

Figure 4. 1 Domain

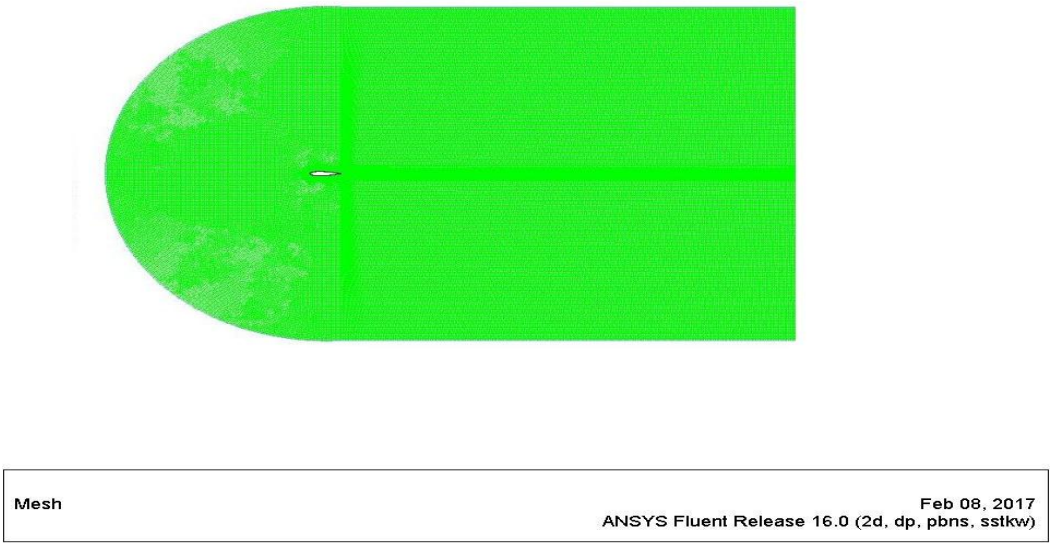

Figure 4. 2 Overview of Mesh

Figure 4.2 represents an overview of mesh to have an overall idea about the mesh where Figure 4.3 shows the close view of unstructured quadrilateral mesh. This figure also shows that the mesh size is smaller near the aerofoil as boundary layer is created near the body and as distance increases the mesh size also increases.

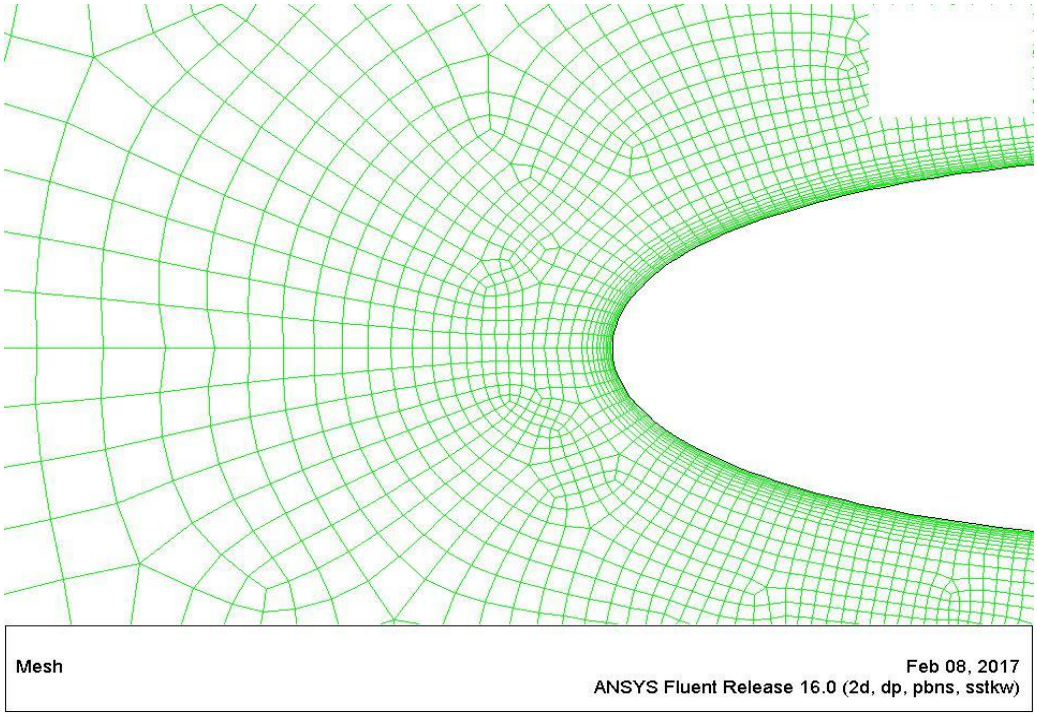

Figure 4. 3 Close view of Mesh

Experimental results of Raghunatah & Ombaka at Re = 2.4 X 10^5 were obtained to validate the simulation results.

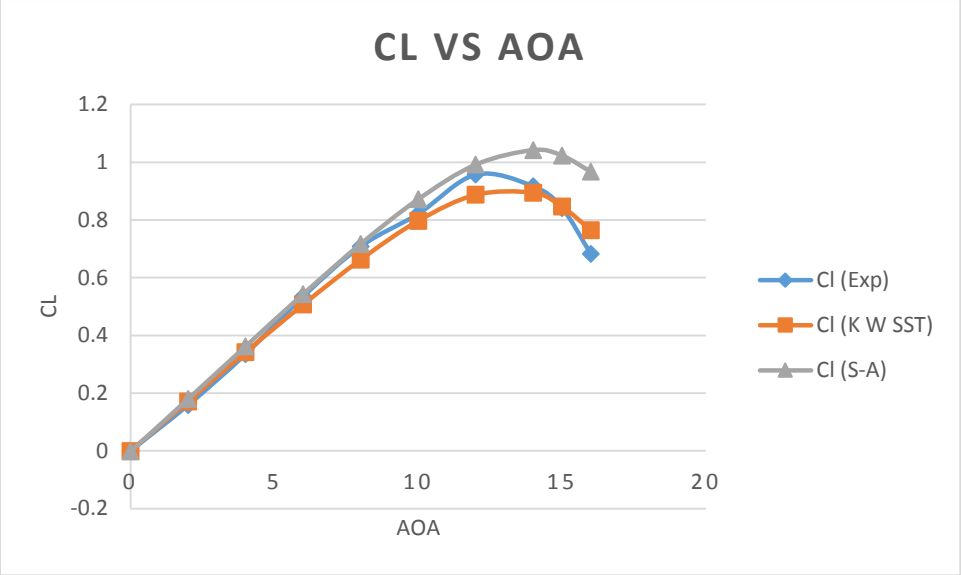

Figure 4. 4 Comparison of C_L curves from experiment & simulation

Figure 4.4 shows the comparative C_L curves where up to 6 degree angle of attack both the simulation models agrees well. After that C_L values obtained from k-w sst deviates a little where C_L values obtained from Spalart Almaras model are still in agreement with the experimental values up to 8 degree angle of attack. After 8 degree angle of attack the experimental values follows a path in between both of the curves obtained from simulation model. Finally, in achieving the C_{Lmax}, k-w sst agrees with experimental values whereas, Spalart Almaras disagrees with the experimental values. Hence, k-ω sst model was used to do the simulations.

4.2 Performance Investigation of NACA 0018 aerofoil through Simulation

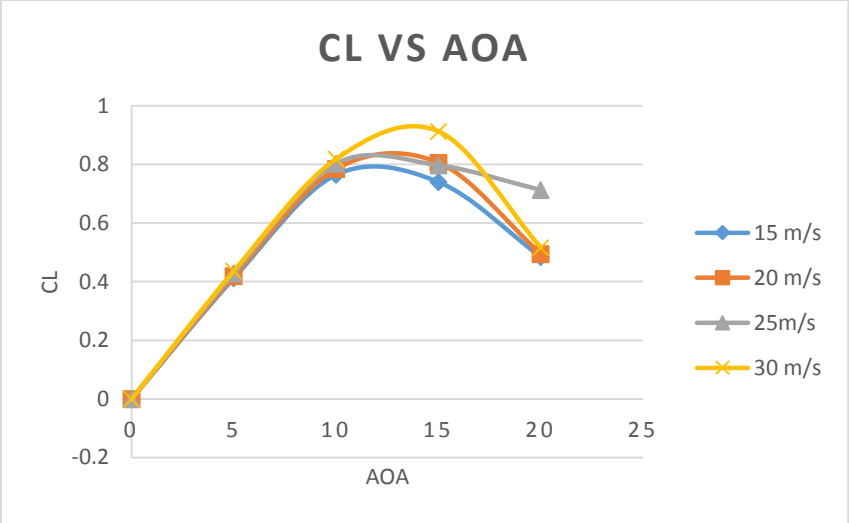

Figure 4. 5 Comparative CL Vs AOA graph at different velocities

This graph shows the lift coefficient curves are very close to each other at the four different velocities all of which follow the same trend. It also shows that maximum value of lift coefficient increases with the increment in velocity.

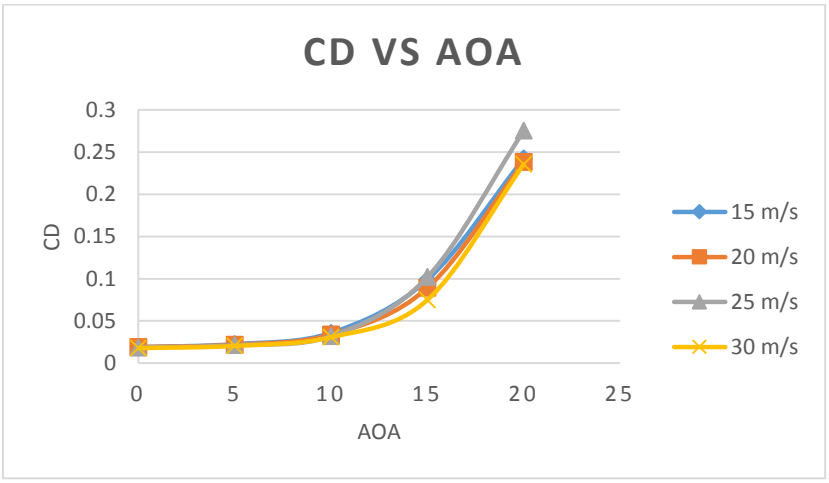

Figure 4. 6 Comparative C_D Vs AOA graph at different velocities

This graph shows the drag coefficient curves are very close to each other at the four different velocities all of which follow the same trend.

4.3 Performance Investigation of Modified NACA 0018 with a cylinder at leading edge

4.3.1 Performance Investigation at V =15 m/s

In all cases, direction of rotation was considered clockwise where the flow direction was from left to right. It was because only this direction of rotation associated with the flow direction could inject momentum on the upper surface of aerofoil.

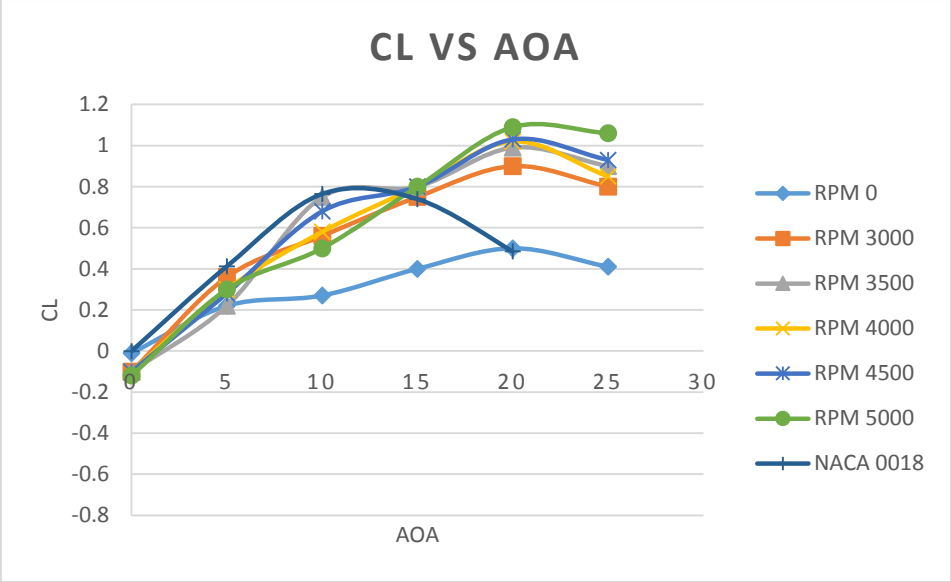

Figure 4. 7 Effect of leading edge rotating cylinder on the lift and stall characteristics of NACA 0018 at various RPM at V= 15 m/s

Figure 4.7 represents the behaviour of modified NACA 0018 aerofoil in terms of lift coefficient and compares it with the behaviour of NACA 0018 aerofoil. The graph shows that performance of modified NACA 0018 degrades at 0 rpm but performance improves with the introduction of rotation. The maximum lift coefficient of modified NACA 0018 increases as the rpm of cylinder increases. As the rpm increases the rotating cylinder at the leading edge it increases the upstream air velocity and forces the air on the upper surface to remain attached. As a result the stall is delayed. From Figure 4.7 it is evident that NACA 0018 aerofoil stalls at around 12 degree at velocity 15 m/s whether modified NACA 0018 aerofoil at the velocity stalls at 20 degree at all rpm starting from 3000 to 5000 with an interval of 500 rpm. It is also clear that as the rpm increases the value of maximum lift coefficient increases. At all rpm maximum lift coefficient is greater than the NACA 0018 aerofoil. As the rpm of the cylinder increases the local air velocity over the upper surface of the aerofoil increases and as the local velocity of air increases the lift coefficient also increases.

At velocity of 15 m/s and at 3000 rpm, the maximum lift coefficient increases by 18.4% compared to the NACA 0018 aerofoil.

At velocity of 15 m/s and at 3500 rpm, the maximum lift coefficient increases by 29.6% compared to the NACA 0018 aerofoil.

At velocity of 15 m/s and at 4000 rpm, the maximum lift coefficient increases by 33.5% compared to the NACA 0018 aerofoil.

At velocity of 15 m/s and at 4500 rpm, the maximum lift coefficient increases by 34.8% compared to the NACA 0018 aerofoil.

At velocity of 15 m/s and at 5000 rpm, the maximum lift coefficient increases by 42.7% compared to the NACA 0018 aerofoil.

From the above results, it is evident that as rpm increases C_{Lmax} also increases. It is because, with the increment in rpm velocity ratio (ratio of tangential velocity of the cylinder to the free stream velocity) increases and as velocity ratio increases momentum injection increases. This increment in momentum causes increment in C_{Lmax}.

So at a velocity of 15 m/s or Reynolds number 1.4 X 10^5 maximum increment in C_{Lmax} takes place at 5000 rpm while the stall angle is delayed from around 12 degree to 20 degree.

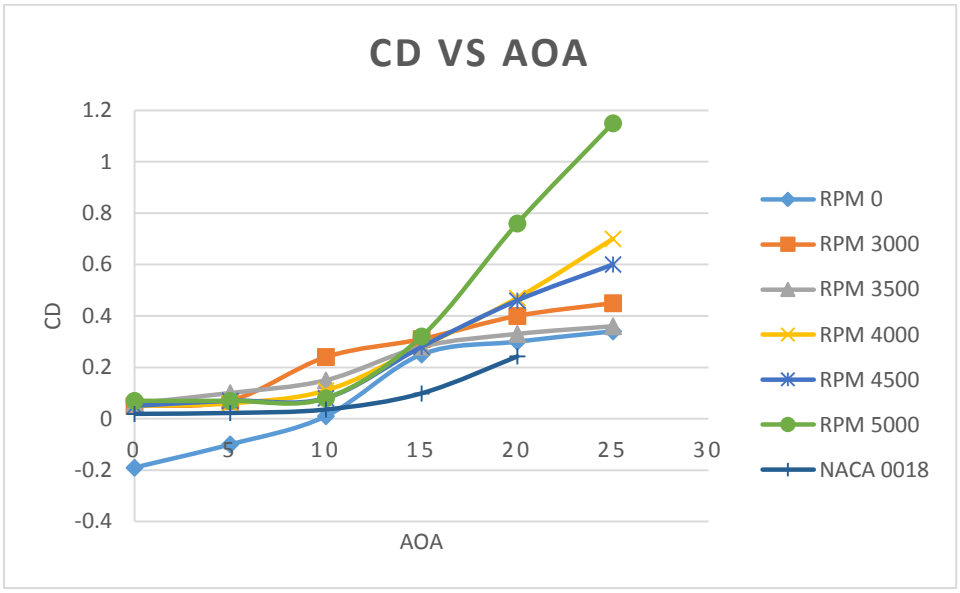

Figure 4. 8 Effect of leading edge rotating cylinder on the drag characteristics of NACA 0018 at various RPM at V= 15 m/s

From Figure 4.8 it can be concluded that in almost all rpm the drag coefficient of modified NACA 0018 increases and as far as drag coefficients are concerned this modified NACA 0018 behaves irregularly.

One phenomena worth of noticing is: at 0 and 5 degree angle of attack at 0 rpm the C_D value is negative. It is anticipated that this occurs due to wake generated behind the cylinder. Because of wake the pressure behind the cylinder is negative and it has a

suction effect on the modified NACA 0018 aerofoil which causes it to have a tendency to move forward as a result of which the drag is negative here.

4.3.2 Performance Investigation at V =20 m/s

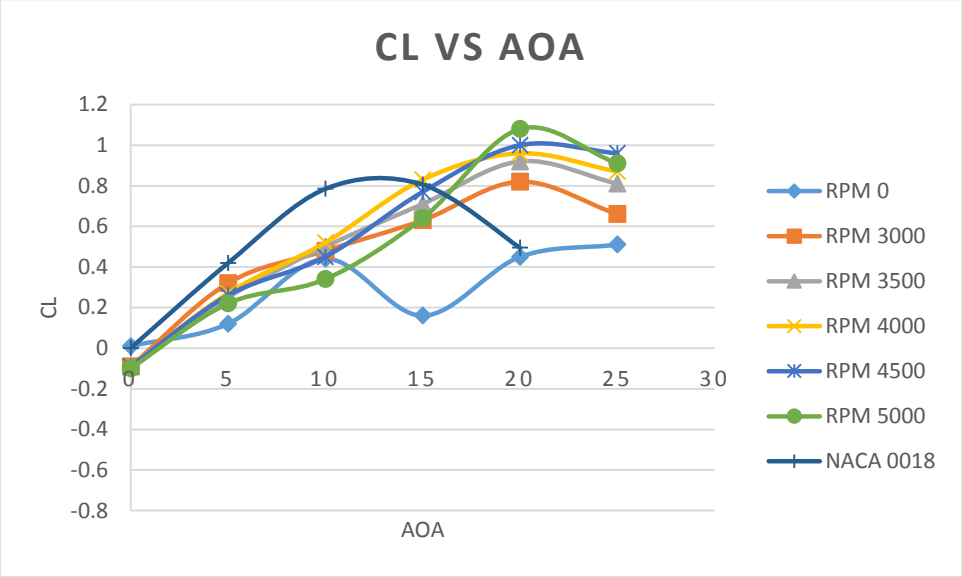

Figure 4. 9 Effect of leading edge rotating cylinder on the lift and stall characteristics of NACA 0018 at various RPM at V= 20 m/s

Figure 4.9 represents the behaviour of modified NACA 0018 aerofoil at 20 m/s velocity in terms of lift coefficient and compares it with the behaviour of NACA 0018 aerofoil. The graph shows that performance of modified NACA 0018 degrades at 0 rpm but performance improves with the introducing of rotation. The maximum lift coefficient of modified NACA 0018 increases as the rpm of cylinder increases. As the rpm increases the rotating cylinder at the leading edge increases the upstream air and forces the air on the upper surface to remain attached. As a result the stall is delayed. From Figure 4.9 it is evident that NACA 0018 aerofoil stalls at around 12 degree at velocity 20 m/s whether modified NACA 0018 aerofoil at the velocity stalls at 20 degree at all rpm starting from 3000 to 5000 with an interval of 500 rpm. It is also clear that as the rpm increases the value of maximum lift coefficient increases. As the rpm of the cylinder increases the local air velocity over the upper surface of the aerofoil increases

and as the local velocity of air increases the lift coefficient also increases.

At velocity of 20 m/s and at 3000 rpm, the maximum lift coefficient increases by 1.86% compared to the NACA 0018 aerofoil.

At velocity of 20 m/s and at 3500 rpm, the maximum lift coefficient increases by 14.3% compared to the NACA 0018 aerofoil.

At velocity of 20 m/s and at 4000 rpm, the maximum lift coefficient increases by 19.25% compared to the NACA 0018 aerofoil.

At velocity of 20 m/s and at 4500 rpm, the maximum lift coefficient increases by 24.2% compared to the NACA 0018 aerofoil.

At velocity of 20 m/s and at 5000 rpm, the maximum lift coefficient increases by 34.16% compared to the NACA 0018 aerofoil.

From the above results, it is evident that as rpm increases C_{Lmax} also increases. It is because, with the increment in rpm velocity ratio (ratio of tangential velocity of the cylinder to the free stream velocity) increases and as velocity ratio increases momentum injection increases. This increment in momentum causes increment in C_{Lmax}.

So at a velocity of 20 m/s or Reynolds number 1.85 X 10^5 maximum increment in Cl_{max} takes place at 5000 rpm while the stall angle is delayed from around 12 degree to 20 degree.

Comparing Figure 4.7 with Figure 4.9 it can be concluded that, at Reynolds number 1.4 X 10^5 the increment in Cl_{max} is greater than that of Reynolds number 1.85 X 10^5.

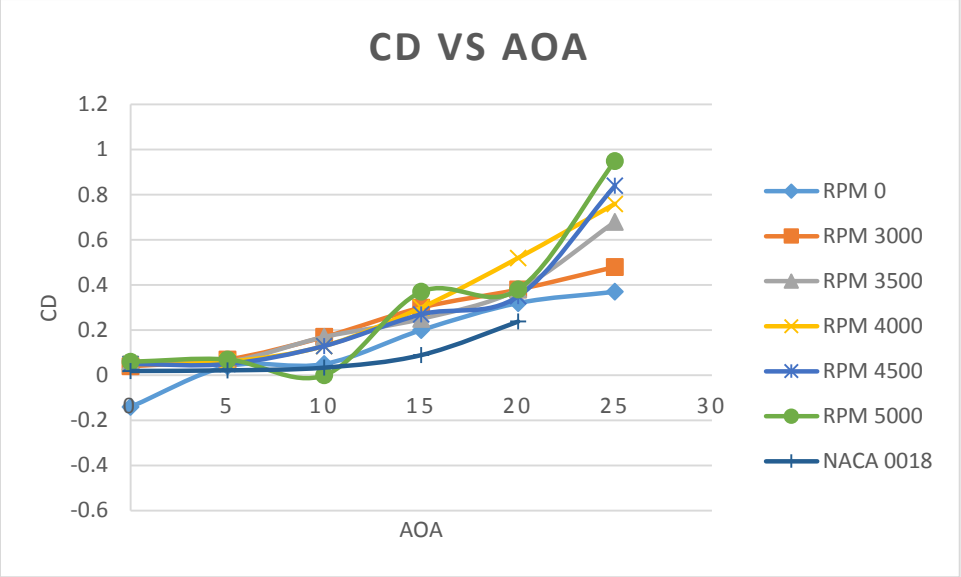

Figure 4. 10 Effect of leading edge rotating cylinder on the drag characteristics of NACA 0018 at various RPM at V= 20 m/s

From Figure 4.10 it can be concluded that in almost all rpm the drag coefficient of modified NACA 0018 increases.

In this case also the coefficient of drag is negative here. It is for the same reason as explain earlier in the case of 15 m/s.

4.3.3 Performance Investigation at V =25 m/s

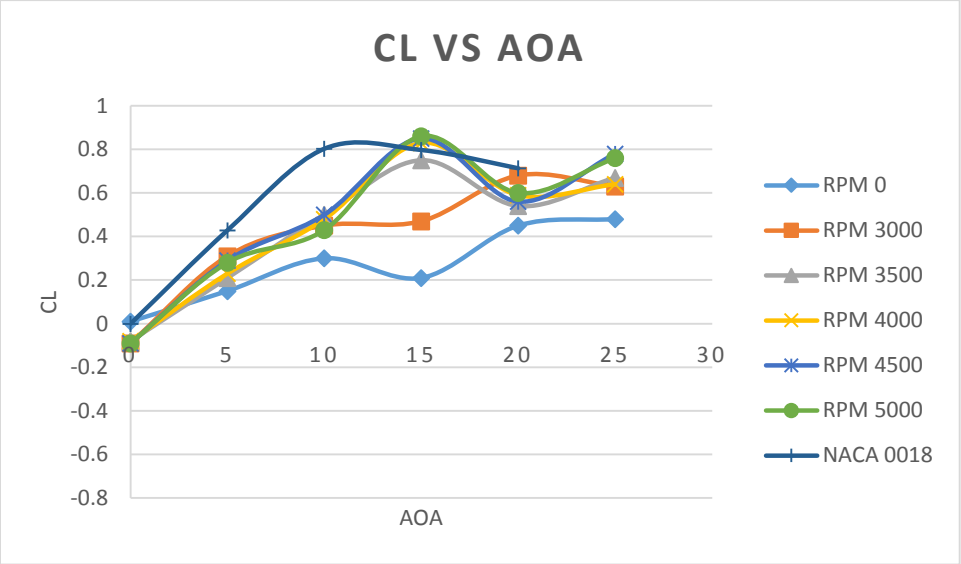

Figure 4. 11 Effect of leading edge rotating cylinder on the lift and stall characteristics of NACA 0018 at various RPM at V= 25 m/s

Even though the modified NACA 0018 aerofoil behaves in a similar manner at Reynolds number 1.4 X 10^5 and 1.85 X 10^5 but Figure 4.11 reveals that its behavior changes at Reynolds number 2.3 X 10^5. It is anticipated that, this occured because of the effect of vibration which becomes predominant at higher velocities.

From Figure 4.11 shows that modified NACA 0018 stalls at 15 degree at Reynolds number 2.3 X 10^5 while it stalled at 20 degree at Reynolds number 1.4 X 10^5 and 1.85 X 10^5 which is a major change in behaviour of modified NACA 0018 aerofoil. In addition to that, unlike the previous Reynolds numbers the Cl_{max} does not surpass the Cl_{max} of NACA 0018 at all rpm rather at this Reynolds number 2.3 X 10^5, only at 4000, 4500 and 5000 rpm the Cl_{max} exceeds the Cl_{max} of NACA 0018 aerofoil while at 0, 3000 and 3500 rpm the Cl_{max} is lower than the Cl_{max} of NACA 0018 aerofoil.

At velocity of 25 m/s and at 4000 rpm, the maximum lift coefficient increases by 3.36% compared to the NACA 0018 aerofoil.

At velocity of 25 m/s and at 4500 rpm, the maximum lift coefficient increases by 5.85% compared to the NACA 0018 aerofoil.

At velocity of 25 m/s and at 5000 rpm, the maximum lift coefficient increases by 7.1% compared to the NACA 0018 aerofoil.

In this case, as free stream velocity has increased to 25 m/s, so the velocity ratio decreases and as the velocity ratio decreases momentum injection decreases. This

decrease in momentum injection causes the stall to occur earlier compared to the previous two Reynolds numbers and decrease in $Cl_{max.}$

So at velocity of 25 m/s or Reynolds number 2.3 X 10^5 maximum increment in Cl_{max} is 7.1% which takes place at 5000 rpm.

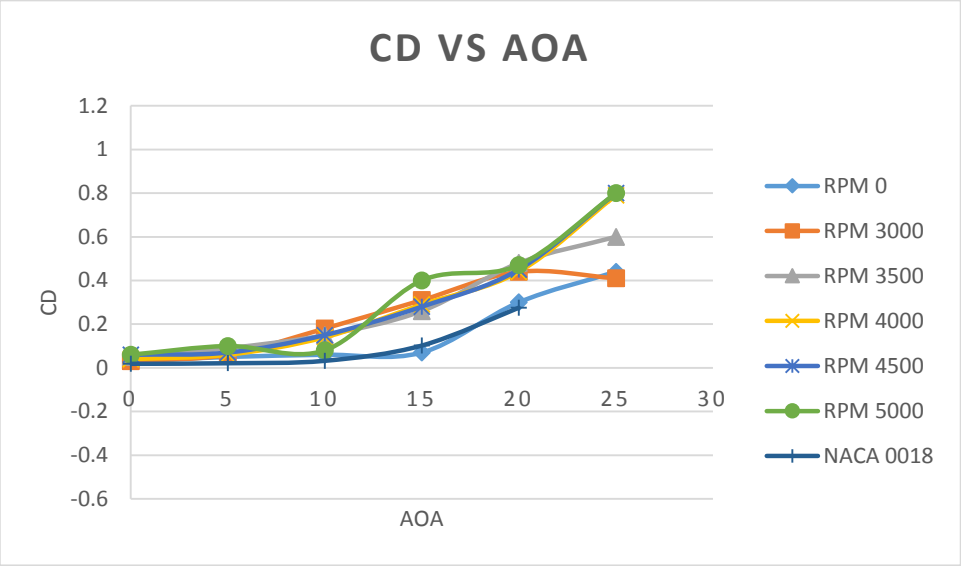

Figure 4. 12 Effect of leading edge rotating cylinder on the drag characteristics of NACA 0018 at various RPM at V= 25 m/s

From Figure 4.12 it can be concluded that in almost all rpm the drag coefficient of modified NACA 0018 increases.

4.3.4 Performance Investigation at V = 30 m/s

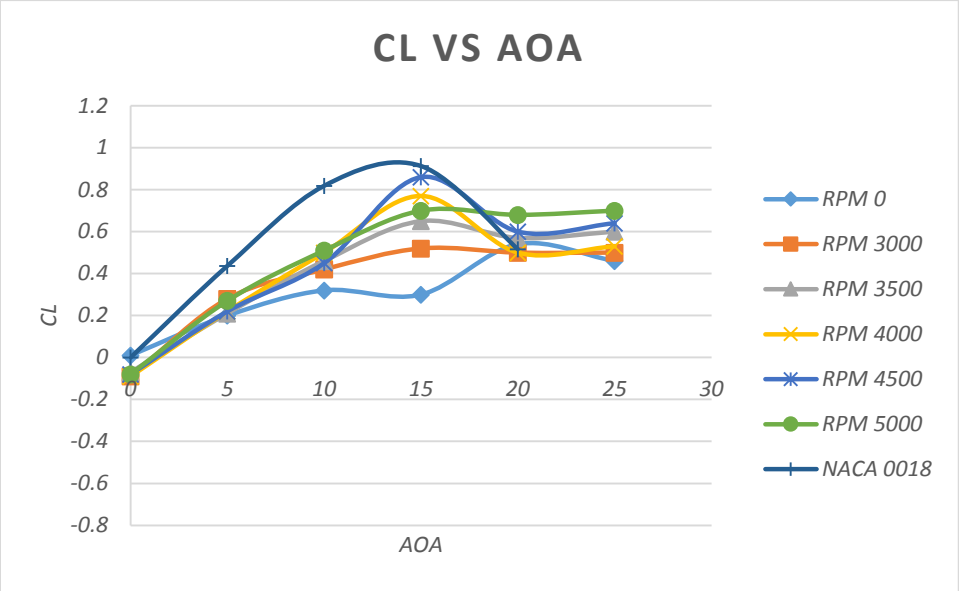

Figure 4. 13 Effect of leading edge rotating cylinder on the lift and stall characteristics of NACA 0018 at various RPM at V= 30 m/s

From Figure 4.13 it is clear that the behaviour of NACA 0018 entirely changes at velocity 30 m/s or at Reynolds number 2.8 X 10^5. Like the Reynolds number 2.3 X 10^5, in this case also the stall occurs at 15 degree. Unlike the behaviour of modified NACA 0018 at Reynolds number 1.4 X 10^5, at this Reynolds number at all rpm the Cl_{max} is much lower than that of the NACA 0018 aerofoil. At this Reynolds number, Cl_{max} increases with the increment in rpm except at 5000 rpm at which Cl_{max} decreases. At this point maximum velocity of the range of this investigation coincides with the maximum rpm which makes the vibration predominant which in turn affects the overall flow pattern, as a result of which Cl_{max} decreases.

In this case, as free stream velocity has increased to 30 m/s, so the velocity ratio decreases and as the velocity ratio decreases momentum injection also decreases. This decrease in momentum injection causes the stall to occur earlier at 15° and decrease in Cl_{max} compared to NACA 0018 aerofoil.

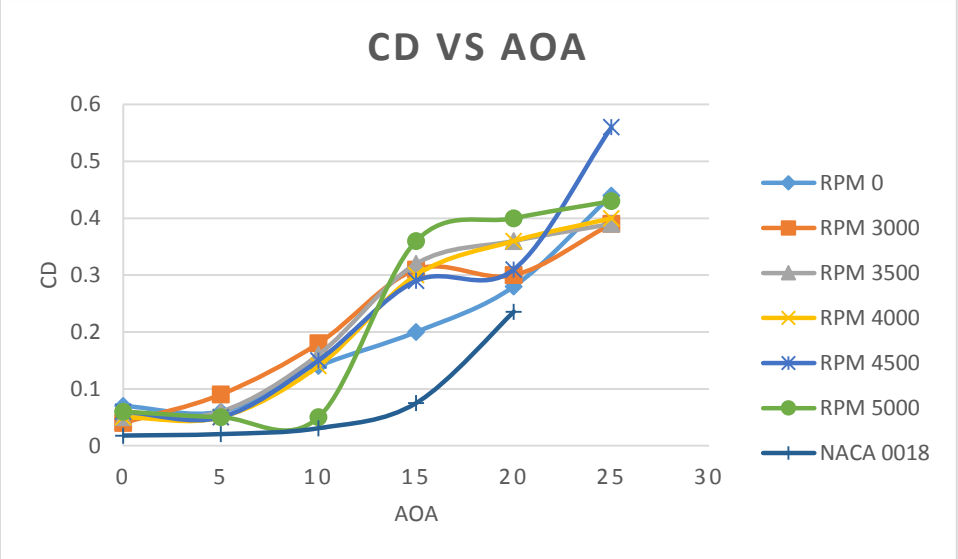

Figure 4. 14 Effect of leading edge rotating cylinder on the drag characteristics of NACA 0018 at various RPM at V= 30 m/s

From Figure 4.14 it can be concluded that in almost all rpm the drag coefficient of modified NACA 0018 increases.

CHAPTER 5

CONCLUSIONS AND RECOMMENDATIONS

5.1 Conclusions

Experiments carried out in this investigation clearly defined the behaviour of modified NACA 0018 at four different Reynolds number 1.4 X 10^5, 1.85 X 10^5, 2.3 X 10^5 and 2.8 X 10^5.

At Reynolds number 1.4 X 10^5: performance of modified NACA 0018 improves both in terms of stall angle and Cl_{max}. Also in this case Cl_{max} gradually increases with the increment in rpm. So, if the requirement of an unmanned aerial vehicle at Reynolds number 1.4 X 10^5 is such that it required stalling to be delayed with a rise in Cl_{max}, then this modified NACA 0018 will serve that purpose. In addition to that basing upon the change in requirement from case to case the Cl_{max} can be varied also.

At Reynolds number 1.85 X 10^5: Like the previous Reynolds number the performance of modified NACA 0018 improves both in terms of stall angle and Cl_{max} in this case. Also in this case Cl_{max} gradually increases with the increment in rpm. So, if the requirement of an unmanned aerial vehicle at Reynolds number 1.85 X 10^5 is such that it required stalling to be delayed with a rise in Cl_{max} like the previous case, then this modified NACA 0018 will serve that purpose. In addition to that basing upon the change in requirement from case to case the Cl_{max} can be varied also.

At Reynolds number 2.3 X 10^5: Unlike the previous cases in this case performance degrades both in terms of stall angle and Cl_{max}. Stalling occurs after 15 degree where the increment in Cl_{max} takes place only at higher rpm namely 4000, 4500 and 5000. If the performance requirement is such that the unmanned aerial vehicle requires to perform variably at Reynolds number 1.85 X 10^5 then this modified NACA 0018 aerofoil will serve the purpose best.

At Reynolds number 2.8 X 10^5: Unlike the previous all cases, in this case Cl_{max} decreases compared to the NACA 0018 aerofoil. If the performance requirement is such that the Cl_{max} is required to lower at all rpm then this modified NACA 0018 aerofoil will serve the purpose best. In this case Cl_{max} increases with the increment in rpm except

the case of 5000 rpm.

Thus it can be concluded that this investigation reveals the performance of modified NACA 0018 aerofoil for the four different Reynolds number. It also demonstrates the way of extracting the advantage of Magnus effect and employing it in serving the performance requirement of unmanned aerial vehicle flying in this regime.

5.2 Limitations

- The groove of the modified NACA 0018 aerofoil was not exactly according to the drawing. Little deviations were there as it was handmade.
- Vibration became predominant at higher rpm and higher velocity.
- Because of the sensitivity of VDAS, values were fluctuating a little bit.
- RPM of the cylinder was not fixed and it was also fluctuating.

5.3 Recommendations for Future Work

- Different regimes of Reynolds number can be investigated to reveal the performance criteria of modified NACA 0018.
- The same investigation may be conducted for different symmetric and asymmetric aerofoil.
- Performance criteria for various aerofoils can be investigated at higher rpm.
- New experimental setup can be built in order to reduce the effect of vibration.
- Doing this same investigation for several aerofoils at same Reynolds number best aerofoil can be chosen against a set of performance requirements through performance optimization.
- Effect of leading edge rotating cylinder on C_m (moment coefficient) may be investigated.
- In present investigation only the forces on aerofoil were taken into consideration. So in future, investigation can be done taking the forces acting on the cylinder into consideration.
- In this investigation the chord length of the modified NACA 0018 aerofoil was taken as 0.15m whereas in practice it was little less than that. So in future investigations the actual length should be taken into consideration.

REFERENCES

[1] John D. Anderson Jr. (2012), Introduction to Flight, 7th Edition, chap 1, pp1, Mc-Graw Hill

[2] John D. Anderson Jr. (1999) , Aircraft Performance and Design, 1st Edition, chap 1, pp17, Mc-Graw Hill

[3] https://airandspace.si.edu/exhibitions/wright-brothes/online/fly/1901

[4] L. J. Clancy (1980), Aerodynamics, 1st Edition, chap 6, pp 112-113 Pitman Publishing Limited

[5] Chang, P.K. (1970), Separation of Flow, 1st Edition, V-170, pp 432, Pergamon,

[6] Lachmann, G.V. (1961), Boundary Layer and Flow Control, 1st Edition, Vols. 1, pp 194, Pergamon

[7] Rosenhead, L. (1966), Laminar Boundary Layers, 1st Edition, pp 486, Oxford University Press

[8] Goldstein, S. (1938), Modern Developments in Fluid Mechanics, 1st Edition, Vols. 1 and 2, pp 531, Oxford University Press.

[9] Schlichting, H. (1979), Boundary Layer Theory, 7th Edition, , pp 38, Mc-Graw-Hill

[10] John D. Anderson Jr. (2008), Fundamentals of Aerodynamics, 4th Edition, pp 64, Mc-Graw Hill,

[11] Modi V. J., Mokhtarian F., 1988**,** Effect of Moving Surfaces **o**n **t**he Airfoil Boundary-Layer Control, Journal of Aircraft, AIAA, 27**-**1, pp 42-50

[12] Mokhtarian F., Modi V. J., 1988, Fluid dynamics of airfoils with moving surface boundary-layer control, Journal of Aircraft, AIAA, 25-2, pp 163-169

[13] Modi V. J., Munshi S. R., Bandyopadhyay G., 1998, High-Performance Airfoil with Moving Surface Boundary Layer Control, Journal of Aircraft, AIAA, 35-4, pp 544-553

[14] Modi V. J., Mokhtarian F., Fernando M. S. U. K., 1997, Moving Surface Boundary-Layer Control as Applied to Two-Dimensional Airfoils, Journal of Aircraft, AIAA, 28-2, pp 104-112

[15] Ahmed Z. Al-Garni, Abdullah M. Al-Garni, Saad A. Ahmed, Ahmet Z. Sahin, 2000, Flow Control for an Airfoil with Leading-Edge Rotation: An Experimental Study, Journal of Aircraft, AIAA, Vol-37, No-4, pp 618-623,

[16] Tayeb Yahiaoui, Mohamed Belhenniche and Bachir Imine, 2015, Effect of Moving Surface on NACA 63218 Aerodynamic Performance, EPJ Web of Conferences, Vol-92, No: 02114

[17] Jost Seifert, 2012, A review of the Magnus effect in aeronautics, Progress in Aerospace Sciences Vol-55 No: 45, pp 17-45

[18] Kavithasan Patkunam, Samay Sigamani, Pedaballi Mahathi, Selvakumaran, Oct-2015, Experimental Study of Magnus Effect over an Aircraft Wing, International Journal of Research in Engineering and Technology, Vol-4, No-10, pp 406-414

[19] Kern E. Kenyon, 2016, On the Magnus Effect, Natural Science, Vol- 8, No: 52, pp 49-52

[20] Timo Sailaranta, 2016, Studies on Unmanned Atmospheric Flight, Doctoral Dissertation, Department of Applied Mechanics, Aalto University, Finland, pp 40

[21] John J. Bertin, Russell M. Cummings (2014), Aerodynamics for Engineers, Pearson International Edition, 6th Edition**,** chap- pp 246

APPENDIX A

Data Tables

Table 3. 1 Actual weight and DRAG cell values

Ser. No.	Actual mass(kg)	Actual wt. (N)	Drag Cell with spring(N)	Zero Reading (N)	Final Value of Drag Cell(N)
1	0	0	-1.09	-1.11	0.02
2	0.5	4.905	3.77	-1.11	4.88
3	1	9.81	8.59	-1.11	9.7
4	1.5	14.715	13.48	-1.11	14.59
5	2	19.62	18.32	-1.11	19.43
6	2.5	24.525	23.21	-1.11	24.32
7	3	29.43	28.03	-1.11	29.14
8	3.5	34.335	32.92	-1.11	34.03
9	4	39.24	37.8	-1.11	38.91
10	4.5	44.145	42.65	-1.11	43.76
11	5	49.05	47.58	-1.11	48.69

Table 3. 2 Actual Weight Vs Final Values of FORE Cell Values

Ser. No.	Actual mass(kg)	Actual wt(N)	Fore Cell(N)	Zero Reading (N)	Final Value of Fore Cell(N)
1	0	0	-21.96	3.27	-25.23
2	0.5	4.905	-17.15	3.27	-20.42
3	1	9.81	-12.18	3.27	-15.45
4	1.5	14.715	-7.2	3.27	-10.47
5	2	19.62	-2.24	3.27	-5.51
6	2.5	24.525	2.68	3.27	-0.59
7	3	29.43	7.63	3.27	4.36
8	3.5	34.335	12.57	3.27	9.3
9	4	39.24	17.51	3.27	14.24
10	4.5	44.145	22.5	3.27	19.23
11	5	49.05	27.47	3.27	24.2

Table 3. 3 Actual Weight Vs Final Values of AFT Cell Values

Ser. No.	Actual mass(kg)	Actual wt(N)	Aft Cell(N)	Zero Reading(N)	Final Value of Aft Cell
1	0	0	-22.76	1.78	-24.54
2	0.5	4.905	-18	1.78	-19.78
3	1	9.81	-13.2	1.78	-14.98
4	1.5	14.715	-8.4	1.78	-10.18
5	2	19.62	-3.6	1.78	-5.38
6	2.5	24.525	1.2	1.78	-0.58
7	3	29.43	6	1.78	4.22
8	3.5	34.335	10.82	1.78	9.04
9	4	39.24	15.62	1.78	13.84
10	4.5	44.145	20.44	1.78	18.66
11	5	49.05	25.25	1.78	23.47

Table 3. 4 Experimental and Ideal values of Cl & Cd of NACA 2412

Alpha	Exp C_l	Ideal C_l	Exp C_d	Ideal C_d
-4	-0.16	-0.166	0.03	0.034
-2	0.006	0.008	0.025	0.03
0	0.229	0.234	0.028	0.03
2	0.45	0.464	0.04	0.032
4	0.7	0.683	0.04	0.04
6	0.9	0.921	0.05	0.053
8	1.07	1.099	0.07	0.072
10	1.2	1.242	0.09	0.085
12	1.3	1.325	0.18	0.155
14	1.16	1.152	0.29	0.279

Table 3. 5 Motor Specifications

Motor ID	**2040SL**
Max Current (A) / Max Vol (V)	20A/12.6V
Maximum Power	0.338 hp
No Load Current (A) @ 7.4V	1.8A
Resistance	0.0399
Diameter	20 mm
Diameter of water cooling pipe	Φ4mm
Length (without Shaft)	40 mm
Shaft Diameter	2.3 mm
Shaft Length	12.5 mm
Weight	60g/2.12oz

Table 4. 1 Comparative CL Vs AOA data table of experiment & simulation data

AOA	Cl (Exp)	Cl (K W SST)	Cl (S-A)
0	0	-0.0002097	-0.00213
2	0.159036	0.17105779	0.179664
4	0.335422	0.34218088	0.362179
6	0.53494	0.50698354	0.543136
8	0.708434	0.66271087	0.717023
10	0.821205	0.79710552	0.871733
12	0.957108	0.88717368	0.991888
4	0.916627	0.89411437	1.0422
15	0.841446	0.84634722	1.023061
16	0.68241	0.76491298	0.967297

Table 4. 2 Values of lift and drag coefficient at various velocities and angles of attack

	Cl				Cd			
alpha	15 m/s	20 m/s	25m/s	30 m/s	15 m/s	20 m/s	25 m/s	30 m/s
0	-0.00029	-0.00014	-0.00022	-0.00021	0.018961	0.019064	0.018477	0.017808
5	0.412188	0.418729	0.428464	0.43672	0.022529	0.021818	0.021194	0.020408
10	0.76461	0.784534	0.802752	0.818444	0.035899	0.033868	0.032118	0.030731
15	0.739884	0.805795	0.796898	0.912575	0.098886	0.089341	0.10196	0.074971
20	0.484561	0.494386	0.712858	0.516388	0.242405	0.238071	0.275279	0.235624

Table 4. 3 Values of lift coefficient at various angles of attack for various RPM at V= 15 m/s

	Cl						
AOA	RPM 0	RPM 3000	RPM 3500	RPM 4000	RPM 4500	RPM 5000	NACA 0018
0	-0.01	-0.1	-0.1	-0.1	-0.1	-0.12	-0.00029
5	0.22	0.36	0.22	0.3	0.28	0.3	0.412188
10	0.27	0.56	0.75	0.58	0.68	0.5	0.76461
15	0.4	0.75	0.8	0.8	0.8	0.8	0.739884
20	0.5	0.9	0.99	1.02	1.03	1.09	0.484561
25	0.41	0.8	0.9	0.85	0.93	1.06	

Table 4. 4 Values of drag coefficient at various angles of attack for various RPM at V = 15 m/s

	Cd						
AOA	RPM 0	RPM 3000	RPM 3500	RPM 4000	RPM 4500	RPM 5000	NACA 0018
0	-0.19	0.05	0.06	0.05	0.05	0.07	0.018961
5	-0.1	0.07	0.1	0.06	0.07	0.07	0.022529
10	0.01	0.24	0.15	0.11	0.08	0.08	0.035899
15	0.25	0.31	0.28	0.28	0.28	0.32	0.098886
20	0.3	0.4	0.33	0.47	0.46	0.76	0.242405
25	0.34	0.45	0.36	0.7	0.6	1.15	

Table 4. 5 Values of lift coefficient at various angles of attack for various RPM at V = 20 m/s

	Cl						
AOA	RPM 0	RPM 3000	RPM 3500	RPM 4000	RPM 4500	RPM 5000	NACA 0018
0	0.01	-0.09	-0.09	-0.09	-0.09	-0.1	-0.00014
5	0.12	0.32	0.25	0.27	0.26	0.22	0.418729
10	0.44	0.48	0.5	0.52	0.45	0.34	0.784534
15	0.16	0.63	0.71	0.83	0.77	0.64	0.805795
20	0.45	0.82	0.92	0.96	1	1.08	0.494386
25	0.51	0.66	0.81	0.87	0.96	0.91	

Table 4. 6 Values of drag coefficient at various angles of attack for various RPM at V=20m/s

	Cd						
AOA	RPM 0	RPM 3000	RPM 3500	RPM 4000	RPM 4500	RPM 5000	NACA 0018
0	-0.14	0.04	0.06	0.05	0.05	0.06	0.01906402
5	0.04	0.07	0.06	0.06	0.05	0.07	0.021818255
10	0.05	0.17	0.17	0.13	0.13	0	0.033867926
15	0.2	0.3	0.25	0.3	0.27	0.37	0.089340582
20	0.32	0.38	0.38	0.52	0.35	0.38	0.238071366
25	0.37	0.48	0.68	0.76	0.84	0.95	

Table 4. 7 Values of lift coefficient at various angles of attack for various RPM at V=25m/s

	Cl						
AOA	RPM 0	RPM 3000	RPM 3500	RPM 4000	RPM 4500	RPM 5000	NACA 0018
0	0.01	-0.09	-0.08	-0.08	-0.09	-0.09	-0.00022
5	0.15	0.31	0.21	0.23	0.29	0.28	0.428464
10	0.3	0.45	0.5	0.48	0.5	0.43	0.802752
15	0.21	0.47	0.75	0.83	0.85	0.86	0.796898
20	0.45	0.68	0.54	0.59	0.56	0.6	0.712858
25	0.48	0.63	0.67	0.64	0.78	0.76	

Table 4. 8 Values of drag coefficient at various angles of attack for various RPM at V=25m/s

	Cd						
AOA	RPM 0	RPM 3000	RPM 3500	RPM 4000	RPM 4500	RPM 5000	NACA 0018
0	0.03	0.03	0.05	0.04	0.06	0.06	0.018477
5	0.05	0.06	0.09	0.06	0.07	0.1	0.021194
10	0.06	0.18	0.15	0.14	0.15	0.08	0.032118
15	0.07	0.31	0.26	0.29	0.28	0.4	0.10196
20	0.3	0.44	0.48	0.44	0.45	0.47	0.275279
25	0.44	0.41	0.6	0.79	0.8	0.8	

Table 4. 9 Values of lift coefficient at various angles of attack for various RPM at V=30m/s

	Cl						
AOA	RPM 0	RPM 3000	RPM 3500	RPM 4000	RPM 4500	RPM 5000	NACA 0018
0	0.01	-0.09	-0.07	-0.09	-0.08	-0.08	-0.000206323
5	0.2	0.28	0.21	0.22	0.22	0.27	0.436720092
10	0.32	0.42	0.46	0.5	0.45	0.51	0.818444016
15	0.3	0.52	0.65	0.77	0.86	0.7	0.912574802
20	0.54	0.5	0.57	0.5	0.6	0.68	0.51638795
25	0.46	0.5	0.6	0.53	0.64	0.7	

Table 4. 10 Values of drag coefficient at various angles of attack for various RPM at V=30m/s

	Cd						
AOA	RPM 0	RPM 3000	RPM 3500	RPM 4000	RPM 4500	RPM 5000	NACA 0018
0	0.07	0.04	0.05	0.05	0.06	0.06	0.017808
5	0.06	0.09	0.06	0.05	0.05	0.05	0.020408
10	0.14	0.18	0.16	0.14	0.15	0.05	0.030731
15	0.2	0.31	0.32	0.3	0.29	0.36	0.074971
20	0.28	0.3	0.36	0.36	0.31	0.4	0.235624
25	0.44	0.39	0.39	0.4	0.56	0.43	